



#### Available online at www.sciencedirect.com

# **ScienceDirect**

Comput. Methods Appl. Mech. Engrg. 393 (2022) 114738

Computer methods in applied mechanics and engineering

www.elsevier.com/locate/cma

# Temporal stability of collocation, Petrov–Galerkin, and other non-symmetric methods in elastodynamics and an energy conserving time integration

Jiarui Wang, Michael C. Hillman\*

Department of Civil and Environmental Engineering, The Pennsylvania State University, University Park, PA 16802, USA

Received 6 November 2021; received in revised form 4 February 2022; accepted 6 February 2022

Available online 14 March 2022

#### Abstract

Non-symmetric matrices may arise in the discretization of self-adjoint problems when a Petrov-Galerkin, collocation, or finite-volume method is employed. While these methods have been widely applied, in this paper it is shown that the use of these non-symmetric matrices is incompatable with the conservation of energy in elastodynamics. First, the consistency between the continuous forms of the momentum equation and the energy equation is examined. It is shown that the conservation of linear momentum is equivalent to conservation of energy provided the solution is sufficiently smooth. The semi-discrete counterparts are then analyzed, where it is demonstrated that they are also equivalent, but only conditionally: the mass and stiffness matrices must be symmetric. As a result, employing a non-symmetric method in elastodynamics may artificially generate or dissipate energy. The fully discrete forms with Newmark time integration are then examined where it is shown that unconditionally unstable algorithms may arise. An energy-conserving time integration algorithm is then proposed which provides stability in the solutions of non-symmetric systems. The collocation and finite-volume methods are employed in numerical examples to demonstrate stability issues and the effectiveness of the proposed time integration methodology.

© 2022 Elsevier B.V. All rights reserved.

Keywords: Collocation; Petrov-Galerkin; Temporal stability; Elastodynamics; Non-symmetric; Energy conservation

## 1. Introduction

The residual-based weak form and collocation of the strong form are the two major branches of numerical approaches in solving elastodynamic problems. The Galerkin type of method is most synonymous with the weak form, which yields symmetric stiffness and mass matrices provided the Bubnov–Galerkin variety (using the same test and trial functions) is employed. This is well-motivated since this ensures coercivity, the best approximation property, and Galerkin orthogonality, at least in the continuous sense (without quadrature) [1,2]. Nevertheless, the development of test functions that differ from trial functions in solid mechanics, termed the Petrov–Galerkin approach, has been driven by several factors including formulation of meshfree (or conforming cell-free) varieties of quadrature [3,4], and constructing variationally consistent integration (passing the patch test) [5–7]. Of course,

E-mail address: mhillman@psu.edu (M.C. Hillman).

<sup>\*</sup> Corresponding author.

these approaches result in non-symmetric, and possibly non-positive-definite matrices which is a popular critique, but usually only from a solver selection standpoint.

Strong form methods, which rely on collocation, discretize the field variables directly in the boundary value problem itself, and facilitate a comparatively simpler numerical approach assembling equations row-by-row [8–12]. These can also be viewed as Petrov–Galerkin methods with a Dirac delta test function, and also yield non-symmetric systems. During the early years of development, the collocation method did not attract much attention from researchers since the compatible finite element approximation cannot achieve higher-order smoothness easily in multiple dimensions, and meanwhile, governing equations of interest are in general at least second-order. However, with the advent of smooth approximation techniques, such as meshfree [13] and isogeometric methodologies [14], there has been a resurgence in collocation methods.

Another set of collocation approaches is the class of finite-volume methods, which can also be considered a Petrov–Galerkin approach. If a Heaviside test function is adopted in the weighted residual, then the local integral forms found in finite-volume methods are recovered over each support [15], also resulting in collocation equations. While more attention has been paid to the standard Galerkin-type approaches in solids over the years, this method has nevertheless been applied successfully for several decades [16]. A well-known implementation for solids is the class of meshless local Petrov–Galerkin methods (MLPGs) [3,17], where a variant "MLPG5" uses a Heaviside test function, yielding non-conforming control volumes [18]. Interestingly, this provides a quite elegant and efficient implementation of meshfree methods for various reasons including simplicity of quadrature, but it MLPG5 did not seem to gain widespread use. Nevertheless, since the test and trial functions differ, the class of finite-volume methods generally result in non-symmetric mass and stiffness matrices in elastodynamics.

While the stability in time of elastodynamic systems using Bubnov-Galerkin methods is well characterized (c.f. [1] for a summary), this does not appear to be the case for non-symmetric systems. Many of the main results rely on the symmetry and positive definiteness of the matrices, which is not guaranteed for this class of numerical methods. Meanwhile, a search of the literature suggests that stability has not been examined closely. While several stable results have been presented for non-symmetric methods in elastodynamics [19–23], that authors believe these are special cases of uniform discretizations where quasi-symmetric matrices have been observed in our studies (later several demonstration problems will be presented). It is well-known by some researchers for instance, meshfree and isogeometric approximations (and discretizations in general) often result in special cases for uniform discretizations [24–31].

In this paper, the important phenomenon of stability in time for non-symmetric methods in elastodynamic systems is analyzed, which is accomplished via continuous, semi-discrete, and fully-discrete energy analyses. The conservation of linear momentum, i.e., the governing equation of elastodynamic problems will be shown to be equivalent to the conservation of energy in the continuous sense, but conditionally equivalent in the semi-discrete sense. The critical ingredient for the equivalency is the symmetricity of the mass and stiffness matrices. In fact, under the conventional symmetric Bubnov–Galerkin approach, the momentum and energy equations are solved simultaneously. Yet on the contrary, when the system matrices are non-symmetric, solving the momentum equation (the governing equation in other words) cannot guarantee the conservation of energy, which finally can lead to to unbounded energy growth in time. It will be demonstrated even under "unconditionally stable" time integration schemes (by conventional knowlege), the non-symmetric type algorithms tend to be unstable, and in fact, can be unconditionally unstable.

An energy conserving time integration algorithm is proposed for elastodynamic problems based on these analyses. The key idea is to equate the discrete energy increment over a time slot to the work done by the external power in the fully-discrete system of equations. This results in an additional energy constraint, used as a supplement to the original system of equations. The reproducing kernel collocation method (RKCM) and reproducing kernel finite-volume method (RKFM) are employed in this study as prototypical non-symmetric approaches to verify the analysis and test the effectiveness of the proposed methodology. As an important detour, the connections between the reproducing kernel collocation and reproducing kernel finite-volume methods will be discussed, followed by a finite volume-type of natural boundary condition enforcement for the standard collocation method to facilitate explicit analysis.

The remainder of this paper is organized as follows: the governing equations and the reproducing kernel approximation are first introduced; the reproducing kernel collocation method (RKCM) and reproducing kernel finite-volume method (RKFM) are then discussed as model non-symmetric methods, as well as the connection

between these two methods. The temporal instability when solving elastodynamic problems using non-symmetric methods is then examined, followed by a newly proposed energy-conserving time integration algorithm. Numerical examples are then provided to demonstrate the effectiveness of the proposed algorithm, followed by conclusions.

#### 2. Model non-symmetric methods for elastodynamics

#### 2.1. Strong form of the momentum equation

In this study, linear elastodynamic problems are considered. The strong form of the balance of linear momentum in continuum mechanics is given over the time interval  $]0, t_f[$  as:

$$\nabla \cdot \boldsymbol{\sigma} + \boldsymbol{b} = \rho \boldsymbol{\ddot{u}} \quad \text{in } \Omega$$

$$\boldsymbol{\sigma} \cdot \boldsymbol{n} = \boldsymbol{\bar{t}} \quad \text{on } \Gamma_h$$

$$\boldsymbol{u} = \boldsymbol{\bar{u}} \quad \text{on } \Gamma_g$$
(1)

where  $\sigma = \mathbb{C}: \varepsilon(u)$  is the Cauchy stress;  $\mathbb{C}$  denotes the isotropic fourth-order elasticity tensor,  $\varepsilon(u) \equiv \frac{1}{2}(\nabla u + (\nabla u)^{\mathsf{T}})$  is the strain tensor, u is the displacement; b is the body force,  $\ddot{u} \equiv d^2 u/dt^2$  denotes the acceleration (following the same notation herein denote the velocity as  $\dot{u} \equiv du/dt$ ), n and  $\bar{t}$  represent the outward normal and the traction on the natural boundary  $\Gamma_h$ , and  $\bar{u}$  is the prescribed displacement on the essential boundary  $\Gamma_g$ . The initial conditions for Eq. (1) in this study are given as:

$$u(x,0) = u_0(x) \text{ in } \Omega$$

$$\dot{u}(x,0) = v_0(x) \text{ in } \Omega$$
(2)

where  $\mathbf{u}_0$  and  $\mathbf{v}_0$  are the initial displacement and velocity, respectively.

## 2.2. Reproducing Kernel (RK) approximation

In this work, the reproducing kernel (RK) [32,33] is employed as a model approximation for the construction of the numerical schemes discussed. The formulation provides sufficient smoothness for both the classical weak-form approaches and the strong-form methods.

Consider a problem domain  $\Omega$  with boundary  $\Gamma$  discretized by a set of NP particles. According to the reproducing kernel methodology, the approximation of field variable u(x, t), denoted by  $u^h(x, t)$  is expressed as follows:

$$\boldsymbol{u}(\boldsymbol{x},t) \approx \boldsymbol{u}^h(\boldsymbol{x},t) = \sum_{I \in \mathcal{S}_{\mathbf{x}}} \Psi_I(\boldsymbol{x}) \boldsymbol{d}_I(t)$$
(3)

where  $d_I$  is a nodal displacement coefficient, and  $\Psi_I(x)$  is the RK shape function associated with the Ith meshfree particle, with a compact support inducing a set of neighbors  $S_x = \{I | \Psi_I(x) \neq 0\}$  local to x. The RK approximation is assumed to take the following form:

$$\Psi_I(x) = \boldsymbol{H}^{\mathsf{T}}(x - x_I)\boldsymbol{b}(x)\phi_a(x - x_I) \tag{4}$$

where  $H(x) = [1, x, y, x^2, \dots, y^p]^T$  is a column vector of complete pth order monomials, b(x) is a column vector containing all the associated unknown coefficients of each component in H, and  $\phi_a(x - x_I)$  is the kernel function with measure a, which defines both the locality and order of smoothness in the approximation. The cubic B-spline function is employed in this work, which possesses  $C^2$  continuity:

$$\phi_a(r) = \frac{1}{6} \begin{cases} (2 - 2r)^3 - 4(1 - 2r)^3 & r \le \frac{1}{2} \\ (2 - 2r)^3 & \frac{1}{2} < r \le 1 \\ 0 & r > 1 \end{cases}$$
 (5)

where  $r \equiv \|\mathbf{x} - \mathbf{x}_I\|/a$  is the normalized relative distance. The unknown coefficient vector  $\mathbf{b}(\mathbf{x})$  is determined by enforcing the following so-called reproducing conditions on the RK shape function  $\Psi(\mathbf{x})$ :

$$\sum_{I \in \mathcal{S}_{\mathbf{x}}} \Psi_I(\mathbf{x}) H(\mathbf{x}_I) = H(\mathbf{x}) \tag{6}$$

which is equivalent to the following shifted basis form:

$$\sum_{I \in S_r} \Psi_I(\mathbf{x}) \mathbf{H}(\mathbf{x} - \mathbf{x}_I) = \mathbf{H}(\mathbf{0}). \tag{7}$$

Then, the unknown coefficient vector b(x) is arrived at by substituting Eq. (4) into Eq. (7), which yields:

$$b(x) = M^{-1}(x)H(0)$$
(8)

where  $M(x) = \sum_{I \in S_x} H(x - x_I) H^T(x - x_I) \phi_a(x - x_I)$  is the so-called moment matrix. Bringing Eq. (8) back into the assumed form of the RK shape function (4), one obtains:

$$\Psi_I(\mathbf{x}) = \mathbf{H}^{\mathsf{T}}(\mathbf{0})\mathbf{M}^{-1}(\mathbf{x})\mathbf{H}(\mathbf{x} - \mathbf{x}_I)\phi_a(\mathbf{x} - \mathbf{x}_I). \tag{9}$$

Note that the order of smoothness of  $\Psi_I(x)$  is inherited given by the kernel function  $\phi_a(x-x_I)$ . Since the cubic spline kernel function employed is  $C^2$ , the shape function is also  $C^2$ , which is favorable for formulations which require higher-order regularity or smoothness such as strong form collocation.

## 2.3. Reproducing Kernel Collocation Method (RKCM)

For the reproducing kernel collocation method [10,12], the key idea is to collocate (evaluate) the governing equations at several points in the domain and on the boundary. The interior points satisfy the governing equation strictly, while points located on the Dirichlet and Neumann boundaries satisfy the corresponding boundary conditions. In this study, the collocation points are selected to be the same location as the meshfree nodes for simplicity (although in practice more collocation points can be chosen for increased accuracy, see [12]). Without loss of generality, for notational simplicity, problems where each node corresponds to a natural or essential boundary are considered, but not both (e.g. a completely fixed, or completely free point). This formulation immediately gives:

$$\rho \ddot{\boldsymbol{u}}(\boldsymbol{x}_I) - \nabla \cdot \boldsymbol{\sigma}(\boldsymbol{x}_I) = \boldsymbol{b}(\boldsymbol{x}_I) \quad \boldsymbol{x}_I \in \Omega$$

$$\boldsymbol{\sigma}(\boldsymbol{x}_I) \cdot \boldsymbol{n} = \bar{\boldsymbol{t}}(\boldsymbol{x}_I) \quad \boldsymbol{x}_I \in \Gamma_h$$

$$\boldsymbol{u}(\boldsymbol{x}_I) = \bar{\boldsymbol{u}}(\boldsymbol{x}_I) \quad \boldsymbol{x}_I \in \Gamma_g$$

$$(10)$$

Substituting the meshfree approximation in Eq. (3) for the field variable of displacement directly into Eq. (10) leads to the following discrete collocation system of equations:

$$\mathbf{M}^C \mathbf{a} + \mathbf{K}^C \mathbf{d} = \mathbf{f}^C \tag{11}$$

where  $\boldsymbol{a}$  and  $\boldsymbol{d}$  are the row vectors of  $\{\ddot{\boldsymbol{d}}_I\}_{I=1}^{NP}$  and  $\{\boldsymbol{d}_I\}_{I=1}^{NP}$ , respectively, with the entries of the matrices and force vector given by:

$$\boldsymbol{M}_{IJ}^{C} = \begin{cases} \boldsymbol{I} \rho [\Psi_{J}(\boldsymbol{x}_{I})] & \boldsymbol{x}_{I} \in \Omega \\ \boldsymbol{0} & \boldsymbol{x}_{I} \in \Gamma_{h} \\ \boldsymbol{0} & \boldsymbol{x}_{I} \in \Gamma_{g} \end{cases}$$
(12)

$$K_{IJ}^{C} = \begin{cases} -\tilde{\nabla}^{\mathsf{T}} C \tilde{\nabla} [\Psi_{J}(\mathbf{x}_{I})] & \mathbf{x}_{I} \in \Omega \\ \Theta^{\mathsf{T}} C \tilde{\nabla} [\Psi_{J}(\mathbf{x}_{I})] & \mathbf{x}_{I} \in \Gamma_{h} \\ I[\Psi_{J}(\mathbf{x}_{I})] & \mathbf{x}_{I} \in \Gamma_{g} \end{cases}$$

$$(13)$$

$$f_{I}^{C} = \begin{cases} b(x_{I}) & x_{I} \in \Omega \\ \bar{t}(x_{I}) & x_{I} \in \Gamma_{h} \\ \bar{u}(x_{I}) & x_{I} \in \Gamma_{g} \end{cases}$$

$$(14)$$

where I is the identity matrix, and 2D cases are considered in this study

$$\tilde{\nabla} = \begin{cases} \frac{\partial}{\partial x} & 0 & \frac{\partial}{\partial y} \\ 0 & \frac{\partial}{\partial y} & \frac{\partial}{\partial x} \end{cases}^{\mathsf{T}} \tag{15}$$

$$\Theta = \begin{bmatrix} n_x & 0 & n_y \\ 0 & n_y & n_x \end{bmatrix}^\mathsf{T} \tag{16}$$

Furthermore, the material matrix is given by the following:

$$C = \frac{\tilde{E}}{1 - \tilde{v}^2} \begin{bmatrix} 1 & \tilde{v} & 0\\ \tilde{v} & 1 & 0\\ 0 & 0 & (1 - \tilde{v})/2 \end{bmatrix}$$
 (17)

where:

$$\tilde{E} = \begin{cases} E & \text{for plane stress} \\ E/(1-v^2) & \text{for plane strain} \end{cases}$$
 (18a)

$$\tilde{\nu} = \begin{cases} \nu & \text{for plane stress} \\ \nu/(1-\nu) & \text{for plane strain} \end{cases}$$
 (18b)

in which E and  $\nu$  are Young's modulus and Poisson's ratio of the material respectively.

In Eqs. (12) and (13), it is seen that the resulting global matrices are not guaranteed to be symmetric by any means, even if the displacement constraints are condensed out of the system.

Although the collocation formulation is straightforward, only static problems can be solved directly without further considerations: for dynamic problems, since no acceleration term is involved in the natural boundary condition relationship, the row equations corresponding to them only contain the displacement field, and the accelerations cannot be directly solved for in the global setting. This aspect of the collocation method will be revisited.

## 2.4. Reproducing Kernel Finite-volume Method (RKFM)

In this section a reproducing kernel finite volume method (RKFM) is introduced, in order to test another prototypical non-symmetric formulation.

First, consider a weighted residual formulation of the strong form in Eq. (1):

$$\int_{\Omega} \boldsymbol{w} \cdot (\rho \ddot{\boldsymbol{u}} - \nabla \cdot \boldsymbol{\sigma} - \boldsymbol{b}) \, d\Omega + \int_{\Gamma_{\boldsymbol{b}}} \boldsymbol{w} \cdot (\boldsymbol{\sigma} \cdot \boldsymbol{n} - \bar{\boldsymbol{t}}) \, d\Gamma = 0.$$
(19)

It is readily shown that the above is equivalent to Eq. (1) provided the essential boundary conditions are enforced strongly on u.

Decomposing the domain into conforming nodal domains associated with each meshfree particle, as illustrated in Fig. 1, the weighted residual formulation in Eq. (19) becomes:

$$\sum_{I=1}^{NP} \int_{\Omega_I} \boldsymbol{w} \cdot (\rho \ddot{\boldsymbol{u}} - \nabla \cdot \boldsymbol{\sigma} - \boldsymbol{b}) \, d\Omega + \int_{\Gamma_I \cap \Gamma_h} \boldsymbol{w} \cdot (\boldsymbol{\sigma} \cdot \boldsymbol{n} - \bar{\boldsymbol{t}}) \, d\Gamma = 0.$$
 (20)

Now, a Heaviside test function is adopted as follows,

$$\boldsymbol{w}(\boldsymbol{x}) \approx \boldsymbol{w}^h(\boldsymbol{x}) = \sum_{I=1}^{NP} \hat{\Psi}_I(\boldsymbol{x}) \boldsymbol{c}_I$$
 (21)

where:

$$\hat{\Psi}_I(\mathbf{x}) = \begin{cases} 1 & \text{when } \mathbf{x} \in \Omega_I \\ 0 & \text{when } \mathbf{x} \notin \Omega_I \end{cases}$$
 (22)

Bringing the Heaviside test function into the weighted residual form in Eq. (20), one has:

$$\int_{\Omega_{I}} (\rho \ddot{\boldsymbol{u}} - \nabla \cdot \boldsymbol{\sigma} - \boldsymbol{b}) \, d\Omega + \int_{\Gamma_{I} \cap \Gamma_{h}} (\boldsymbol{\sigma} \cdot \boldsymbol{n} - \overline{\boldsymbol{t}}) \, d\Gamma = \boldsymbol{0} \quad \Gamma_{I} \cap \Gamma_{g} = \emptyset 
\boldsymbol{u} = \overline{\boldsymbol{u}} \qquad \qquad \Gamma_{I} \cap \Gamma_{g} \neq \emptyset$$
(23)

Invoking the divergence theorem on the stress terms, the reproducing kernel finite volume formulation reads as follows:

$$\int_{\Omega_{I}} \rho \ddot{\boldsymbol{u}} \, d\Omega - \int_{\Gamma_{I}} \boldsymbol{\sigma} \cdot \boldsymbol{n} \, d\Gamma = \int_{\Omega_{I}} \boldsymbol{b} \, d\Omega \qquad \Gamma_{I} \cap \left( \Gamma_{g} \cup \Gamma_{h} \right) = \emptyset$$

$$\int_{\Omega_{I}} \rho \ddot{\boldsymbol{u}} \, d\Omega - \int_{\Gamma_{I} \setminus \left( \Gamma_{I} \cap \Gamma_{h} \right)} \boldsymbol{\sigma} \cdot \boldsymbol{n} \, d\Gamma = \int_{\Gamma_{I} \cap \Gamma_{h}} \tilde{\boldsymbol{t}} \, d\Gamma + \int_{\Omega_{I}} \boldsymbol{b} \, d\Omega \qquad \Gamma_{I} \cap \Gamma_{h} \neq \emptyset$$

$$\boldsymbol{u} = \bar{\boldsymbol{u}} \qquad \Gamma_{I} \cap \Gamma_{g} \neq \emptyset$$
(24)

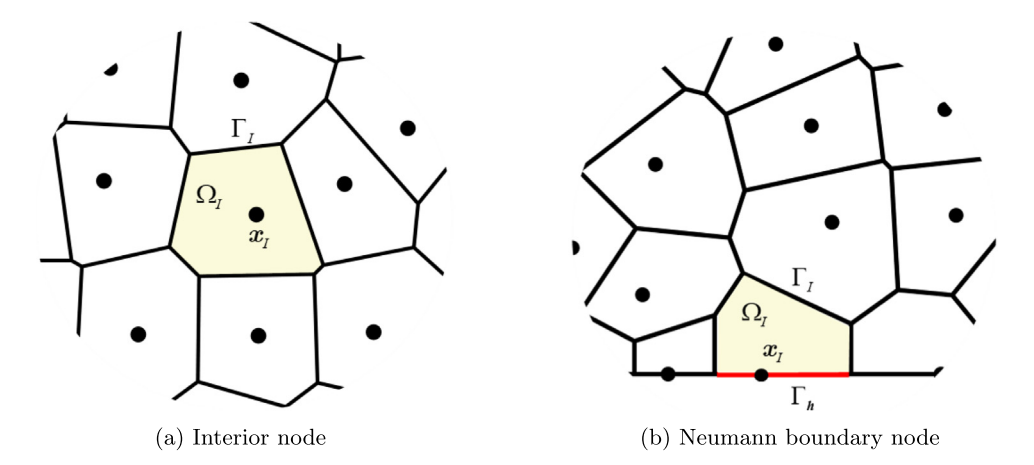


Fig. 1. A conforming domain decomposition using a Voronoi diagram.

As can be seen above, there are three cases in Eq. (24). The first row states the RKFM formulation of an interior node, where the boundary of the particle does not intersect with the total boundary of the domain (see Fig. 1(a)). The second row of Eq. (24) denotes the RKFM formulation for a Neumann particle (see Fig. 1(b)), where the particle boundary has an intersection with the Neumann boundary. Thus, the force contributed from the traction to the particle has been moved to the right hand side. The last row represents a Dirichlet boundary node, which has no difference with the traditional collocation formulation.

The matrix form of the reproducing kernel finite volume method is achieved after substituting trial function approximated by the RK shape function Eq. (3) into Eq. (24):

$$\mathbf{M}^F \mathbf{a} + \mathbf{K}^F \mathbf{d} = \mathbf{F}^F \tag{25}$$

where:

$$\boldsymbol{M}_{IJ}^{F} = \begin{cases} \int_{\Omega_{I}} \boldsymbol{I} \rho \left[ \Psi_{J}(\boldsymbol{x}) \right] d\Omega & \Gamma_{I} \cap \left( \Gamma_{g} \cup \Gamma_{h} \right) = \emptyset \\ \int_{\Omega_{I}} \boldsymbol{I} \rho \left[ \Psi_{J}(\boldsymbol{x}) \right] d\Omega & \Gamma_{I} \cap \Gamma_{h} \neq \emptyset \\ \boldsymbol{0} & \Gamma_{I} \cap \Gamma_{g} \neq \emptyset \end{cases}$$
(26)

$$\mathbf{M}_{IJ}^{F} = \begin{cases}
\int_{\Omega_{I}} \mathbf{I} \rho \left[ \Psi_{J}(\mathbf{x}) \right] d\Omega & \Gamma_{I} \cap \left( \Gamma_{g} \cup \Gamma_{h} \right) = \emptyset \\
\int_{\Omega_{I}} \mathbf{I} \rho \left[ \Psi_{J}(\mathbf{x}) \right] d\Omega & \Gamma_{I} \cap \Gamma_{h} \neq \emptyset \\
\mathbf{0} & \Gamma_{I} \cap \Gamma_{g} \neq \emptyset
\end{cases}$$

$$\mathbf{K}_{IJ}^{F} = \begin{cases}
-\int_{\Gamma_{I}} \Theta^{\mathsf{T}} \mathbf{C} \tilde{\nabla} \Psi_{J} d\Gamma & \Gamma_{I} \cap \left( \Gamma_{g} \cup \Gamma_{h} \right) = \emptyset \\
-\int_{\Gamma_{I} \setminus \left( \Gamma_{I} \cap \Gamma_{h} \right)} \Theta^{\mathsf{T}} \mathbf{C} \tilde{\nabla} \Psi_{J} d\Omega & \Gamma_{I} \cap \Gamma_{h} \neq \emptyset \\
\mathbf{I} \left[ \Psi_{J}(\mathbf{x}_{I}) \right] & \Gamma_{I} \cap \Gamma_{g} \neq \emptyset
\end{cases}$$
(26)

and:

$$\boldsymbol{f}_{I}^{F} = \begin{cases} \int_{\Omega_{I}} \boldsymbol{b} \, d\Omega & \Gamma_{I} \cap \left(\Gamma_{g} \cup \Gamma_{h}\right) = \emptyset \\ \int_{\Gamma_{I} \cap \Gamma_{h}} \bar{\boldsymbol{t}} \, d\Gamma + \int_{\Omega_{I}} \boldsymbol{b} \, d\Omega & \Gamma_{I} \cap \Gamma_{h} \neq \emptyset \\ \bar{\boldsymbol{u}} \left(\boldsymbol{x}_{I}\right) & \Gamma_{I} \cap \Gamma_{g} \neq \emptyset \end{cases}$$

$$(28)$$

It can be clearly seen from Eqs. (26) and (27), due to the collocated type of weighted residual formulation, the stiffness and mass matrices are no longer guaranteed to yield symmetricity.

The simplicity of enforcing a Neumann boundary condition in RKFM can be seen in Eq. (28). In contrast to the condition in RKCM (14), RKFM enables Galerkin-type enforcement Neumann boundary conditions, i.e. the traction is assembled simply into the row equations.

Although one can use the row-sum [1] technique to diagonalize the mass matrix (and hence make it symmetric), the system as a whole will still be non-symmetric since the stiffness matrix remains unchanged.

**Remark 1.** It can be noted from the RKFM weak form that no second-order derivatives of the reproducing kernel approximation are needed, as a result of divergence theorem, which converts the volume integral (with a 2nd order type integrand) to a surface integral (a 1st order type integrand). Thus, the use of only linear RK shape functions (as opposed to quadratic basis needed for convergence in pure collocation [12]) can yield 2nd order convergence rates in space, which makes the RKFM a superconvergent method [28].

**Remark 2.** The equations of RKFM can be directly identified as the conservation of linear momentum of each cell, or Newton's first and second laws, which is a common feature of finite volume methods.

**Remark 3.** Since the tractions on neighboring cell surfaces are equal and opposite by using the smooth RK approximation in conjunction with the conforming cell domain decomposition, Newton's third law is also embedded in the formulation. These observations yield yet another clear physical interpretation of this method.

**Remark 4.** The essential boundary conditions are directly imposed by collocation and the method does not require the special treatments necessary in typical Galerkin meshfree methods.

**Remark 5.** The formulation can be shown to satisfy the variationally consistent integration conditions [6] as a result of using Heaviside test functions. In [6] it was shown that the consistency conditions are an integration-by-parts formula on the test function and a polynomial solution. Here, with the use of a Heaviside function, this is trivially achieved. For example, one point quadrature for all domain and boundary terms satisfies these conditions up to second order. Thus, no accuracy or optimal convergence is lost according to [34].

All of the unique properties listed in these remarks, along with a more detailed presentation of this method will be given in a forthcoming paper by the authors.

#### 2.5. Connection between RKCM and RKFM

In order to evaluate the RKFM semi-discrete form (25), numerical quadrature needs to be carried out. For the finite volume formulation with respect to the interior cells in Eq. (24), direct nodal integration [35] is employed to carry out the numerical evaluation. One point quadrature is also employed for each contour integral.

Then, if one premultiplies by  $1/V_I$ , then the following is obtained:

$$0 = \frac{1}{V_{I}} \left( \int_{\Omega_{I}} \rho \ddot{\boldsymbol{u}} \, d\Omega - \int_{\Gamma_{I}} \boldsymbol{\sigma} \cdot \boldsymbol{n} \, d\Gamma - \int_{\Omega_{I}} \boldsymbol{b} \, d\Omega \right)$$

$$\approx \frac{1}{V_{I}} \left[ V_{I} \rho \ddot{\boldsymbol{u}} \left( \boldsymbol{x}_{I} \right) - \int_{\Gamma_{I}} \boldsymbol{\sigma} \cdot \boldsymbol{n} \, d\Gamma - V_{I} \boldsymbol{b} \left( \boldsymbol{x}_{I} \right) \right]$$

$$= \rho \ddot{\boldsymbol{u}} \left( \boldsymbol{x}_{I} \right) - \frac{1}{V_{I}} \int_{\Gamma_{I}} \boldsymbol{\sigma} \cdot \boldsymbol{n} \, d\Gamma - \boldsymbol{b} \left( \boldsymbol{x}_{I} \right)$$

$$(29)$$

Comparing Eq. (29) with Eq. (10), the following relationship between RKCM and RKFM can clearly be seen:

$$\nabla \cdot \boldsymbol{\sigma}(\boldsymbol{x}_I) \approx \frac{1}{V_I} \int_{\Gamma_I} \boldsymbol{\sigma}(\boldsymbol{x}) \cdot \boldsymbol{n} \, d\Gamma. \tag{30}$$

From Eq. (30), the reproducing kernel finite volume method can be interpreted as applying stress smoothing in the decomposed domain, which will eventually lead to a gradient smoothing procedure similar to stabilized conforming nodal integration [36]. On the other hand, the collocation equation can be obtained if one takes nodal integration on the finite volume equation before applying the divergence theorem in Eq. (23).

#### 2.6. Alternative strategy for the employment of Neumann boundary conditions in RKCM

Although the enforcement of Neumann boundary conditions in a collocation method is non-trivial for dynamic problems, the connection between RKCM and RKFM enables a finite-volume type enforcement in the RKCM formulation. Namely, the Neumann boundary condition for the collocation method can be enforced approximately with the finite-volume technique. For a particle associated with Neumann boundary, the system of collocation equations requires:

$$\rho \ddot{\boldsymbol{u}}(\boldsymbol{x}_I) - \frac{1}{V_I} \int_{\Gamma_I \setminus (\Gamma_I \cap \Gamma_h)} \boldsymbol{\sigma} \cdot \boldsymbol{n} \, d\Gamma = \frac{1}{V_I} \int_{\Gamma_I \cap \Gamma_h} \bar{\boldsymbol{t}} \, d\Gamma + \boldsymbol{b}(\boldsymbol{x}_I). \tag{31}$$

Eq. (31) states an alternative strategy for the employment of Neumann boundary condition in RKCM. Different from the standard collocation formulation, the acceleration term is included in Eq. (31), which is favorable for the numerical implementation, especially for the explicit formulation of elastodynamic problems.

## 3. Temporal instability in solving elastodynamics with non-symmetric numerical methods

#### 3.1. Energy and momentum equations

The temporal stability of non-symmetric systems will first be examined from an energy point of view. Consider the following work-energy potential of a mechanical system:

$$\Pi = K(\dot{\boldsymbol{u}}) + E(\boldsymbol{u}) - P(\boldsymbol{u}) \tag{32}$$

where  $K(\dot{u})$ , E(u) and P(u) represent the kinetic energy, potential energy, and work done by the external forces, respectively:

$$K(\dot{\boldsymbol{u}}) = \int_{\Omega} \frac{1}{2} \rho \dot{\boldsymbol{u}} \cdot \dot{\boldsymbol{u}} \, d\Omega \tag{33}$$

$$E(\mathbf{u}) = \int_{\Omega} \frac{1}{2} \sigma(\mathbf{u}) : \mathbf{\varepsilon}(\mathbf{u}) \, d\Omega \tag{34}$$

$$P(\boldsymbol{u}) = \int_{\Omega} \boldsymbol{b} \cdot \boldsymbol{u} \, d\Omega + \int_{\Gamma_{\boldsymbol{b}}} \bar{\boldsymbol{t}} \cdot \boldsymbol{u} \, d\Gamma \tag{35}$$

According to the conservation of energy, without considering energy dissipation, the following relationship holds since  $\mathbb{C}$  has major symmetry:

$$\dot{\Pi} = \dot{K}(\dot{\boldsymbol{u}}) + \dot{E}(\boldsymbol{u}) - \dot{P}(\boldsymbol{u})$$

$$= \int_{\Omega} \rho \dot{\boldsymbol{u}} \cdot \ddot{\boldsymbol{u}} \, d\Omega + \int_{\Omega} \boldsymbol{\sigma}(\boldsymbol{u}) : \boldsymbol{\varepsilon}(\dot{\boldsymbol{u}}) \, d\Omega - \int_{\Omega} \boldsymbol{b} \cdot \dot{\boldsymbol{u}} \, d\Omega - \int_{\Gamma_h} \bar{\boldsymbol{t}} \cdot \dot{\boldsymbol{u}} \, d\Gamma$$

$$= 0. \tag{36}$$

In Eq. (36), the left-hand side denotes the energy rate, which should be zero in order to satisfy the conservation of energy.

**Remark 6.** In Eq. (36), to simplify the derivation, the body force  $\boldsymbol{b}$  and traction  $\bar{\boldsymbol{t}}$  are assumed independent of time  $\boldsymbol{t}$ . In the general case, one will have the power defined as  $\bar{P}(\dot{\boldsymbol{u}}) = \int_{\Omega} \dot{\boldsymbol{u}} \cdot \boldsymbol{b} \ d\Omega + \int_{\Gamma_h} \dot{\boldsymbol{u}} \cdot \bar{\boldsymbol{t}} \ d\Gamma$ , then the conservation of energy requires:

$$\dot{K}(\dot{\boldsymbol{u}}) + \dot{E}(\boldsymbol{u}) = \bar{P}(\dot{\boldsymbol{u}}) \tag{37}$$

which will eventually yield the same formulation as Eq. (36).

Then, provided the terms in Eq. (36) are smooth enough, performing the integration by parts on the potential energy rate term immediately gives:

$$\dot{\Pi} = \int_{\Omega} \rho \dot{\boldsymbol{u}} \cdot \ddot{\boldsymbol{u}} \, d\Omega + \int_{\Gamma} \dot{\boldsymbol{u}} \cdot (\boldsymbol{\sigma} \cdot \boldsymbol{n}) \, d\Omega 
- \int_{\Omega} \dot{\boldsymbol{u}} \cdot \nabla \cdot \boldsymbol{\sigma} \, d\Omega - \int_{\Omega} \boldsymbol{b} \cdot \dot{\boldsymbol{u}} \, d\Omega - \int_{\Gamma_h} \bar{\boldsymbol{t}} \cdot \dot{\boldsymbol{u}} \, d\Gamma 
= 0$$
(38)

Assuming a fixed essential boundary condition, which implies  $\dot{u} = 0$  on  $\Gamma_g$ , the energy rate can be rewritten as:

$$\int_{\Omega} \dot{\boldsymbol{u}} \cdot (\rho \ddot{\boldsymbol{u}} - \nabla \cdot \boldsymbol{\sigma} - \boldsymbol{b}) \, d\Omega + \int_{\Gamma_h} \dot{\boldsymbol{u}} \cdot (\boldsymbol{\sigma} \cdot \boldsymbol{n} - \bar{\boldsymbol{t}}) \, d\Omega = 0.$$
(39)

Thus, for  $\forall \dot{u}$ , Eq. (39) directly leads to the strong form of elastodynamics problem:

$$\nabla \cdot \boldsymbol{\sigma} + \boldsymbol{b} = \rho \ddot{\boldsymbol{u}}$$

$$\boldsymbol{\sigma} \cdot \boldsymbol{n} = \bar{\boldsymbol{t}}$$
(40)

which is also the conservation of linear momentum.

From the above derivation, it can be seen that the conservation of energy and linear momentum are equivalent in the continuous sense, with only the assumption of continuous stresses and that  $\dot{u} = 0$  on  $\Gamma_g$ . That is, the conservation of energy yields the conservation of linear momentum, while it can be shown that the opposite is also true by working backwards.

## 3.2. Semi-discrete energy analysis

By introducing an approximation of the field variable u through various methods, the matrix form of the momentum Eq. (40) becomes:

$$Ma + Kd = F \tag{41}$$

where M and K denote generic mass and stiffness matrices; at this point, the solution strategy is not specified, which means it can be a Bubnov-Galerkin approximation, Petrov-Galerkin approximation or collocation discretization. In the end, all will result Eq. (41). Importantly, these matrices can be either symmetric and non-symmetric. On the other hand, the numerical version of energy potential in (32), denoted by  $\bar{I}I$  is calculated as:

$$\bar{\Pi} = \frac{1}{2} \mathbf{v}^\mathsf{T} \mathbf{M} \mathbf{v} + \frac{1}{2} \mathbf{d}^\mathsf{T} \mathbf{K} \mathbf{d} - \mathbf{d}^\mathsf{T} \mathbf{F}$$
 (42)

where v is the row vector of  $\{\dot{\boldsymbol{d}}_I\}_{I=1}^{NP}$ .

Next, the numerical energy rate in the semi-discrete sense can be obtained by taking the direct time derivative of Eq. (42). To facilitate the conservation of energy in the semi-discrete level, the energy rate needs to be zero in the numerical sense, i.e.:

$$\dot{\bar{I}} = \frac{1}{2} \dot{v}^{\mathsf{T}} M v + \frac{1}{2} v^{\mathsf{T}} M \dot{v} + \frac{1}{2} \dot{d}^{\mathsf{T}} K d + \frac{1}{2} d^{\mathsf{T}} K \dot{d} - \dot{d}^{\mathsf{T}} F 
= \frac{1}{2} a^{\mathsf{T}} M v + \frac{1}{2} v^{\mathsf{T}} M a + \frac{1}{2} v^{\mathsf{T}} K d + \frac{1}{2} d^{\mathsf{T}} K v - v^{\mathsf{T}} F 
= \frac{1}{2} v^{\mathsf{T}} (M + M^{\mathsf{T}}) a + \frac{1}{2} v^{\mathsf{T}} (K + K^{\mathsf{T}}) d - v^{\mathsf{T}} F 
= v^{\mathsf{T}} \{ \frac{1}{2} (M + M^{\mathsf{T}}) a + \frac{1}{2} (K + K^{\mathsf{T}}) d - F \} 
= 0.$$
(43)

The following relationship guarantees Eq. (43) is satisfied regardless of the choice of v:

$$\frac{1}{2}(M + M^{\mathsf{T}})a + \frac{1}{2}(K + K^{\mathsf{T}})d = F. \tag{44}$$

In summary, the semi-discrete equations for elastodynamic problems are two-fold:

$$Ma + Kd = F$$
 for momentum conservation (45a)

$$\frac{1}{2}(M + M^{\mathsf{T}})a + \frac{1}{2}(K + K^{\mathsf{T}})d = F \quad \text{for energy conservation}$$
 (45b)

According to Eqs. (45a) and (45b), the discrete momentum conservation Eq. (45a) does not take the same form as the discrete energy conservation Eq. (45b). However, in the continuous case discussed earlier, the energy conservation yields the same formulation as the conservation of linear momentum. Therefore, there exists a numerical inconsistency on the semi-discrete level comparing Eqs. (41) and (44). Subsequently, when solving the conservation of linear momentum equation (45a), the conservation of energy requirement may not be satisfied in the numerical procedure.

Because of the equivalency of momentum and energy conservation law in the continuous sense, for the discrete case, the only condition to make the formulas in Eqs. (45a) and (45b) consistent (i.e., the only way both are solved simultaneously) is:

$$K = K^{\mathsf{T}} \tag{46a}$$

$$M = M^{\mathsf{T}} \tag{46b}$$

With the aid of Eq. (46), Eq. (45a) and (45b) reduce to:

$$Ma + Kd = F$$
 for momentum conservation (47a)

$$Ma + Kd = F$$
 for energy conservation (47b)

The importance of symmetricity in formulating stiffness and mass has been demonstrated in Eqs. (47a) and (47b). A symmetric K and M will result in the semi-discrete conservation of energy when the semi-discrete conservation of linear momentum is satisfied.

In summary, a numerical inconsistency has been observed in the semi-discrete level of energy analysis. When a discretization leads to a non-symmetric stiffness matrix K and mass matrix M, which will be true in the general case of any Petrov-Galerkin or collocation method, the conservation of energy is a separate set of equations and distinct from the momentum equations. While a lumped mass can facilitate the symmetricity of M, unless  $K = K^T$  the equations will not be equivalent: the solution of the momentum equation in non-symmetric methods will not satisfy the conservation of energy.

**Remark 7.** It is interesting to note that the employment of non-symmetric matrices results in systems which do not exhibit proper physical behavior, despite being derived from the momentum equations: both the differential form of the momentum equation (as used in Petrov–Galerkin, and collocation), and the integral form (as used in the finite-volume method) can result in these non-physical systems. To the point: if a system could be physically built with the same stiffness properties, it could produce the generation of energy without external forces.

**Remark 8.** The symmetry of the stiffness matrix is synonymous with the Maxwell–Betti law of reciprocal deflection. Therefore this seemingly benign (and non-intuitive), yet useful physical law, has grave implications for discrete elastodynamic systems.

#### 3.3. Fully discrete energy analysis

The semi-discrete energy analysis for non-symmetric systems is provided in the previous subsection. Now, consider the fully discrete energy of elastodynamic systems using the Newmark method [37], which encompasses several popular time integration algorithms as special cases, including the average acceleration and central difference methods. For simplicity, the free vibration case is utilized, where it is easily shown that the fully discrete system violates the condition of zero dissipation in the physical system in the absence of damping.

The first equation in the Newmark approach is the equilibrium equation collocated at a given time  $t_n$ . Let  $d_n$ ,  $v_n$ , and  $a_n$  denote the approximations of  $d(t_n)$ ,  $\dot{d}(t_n)$ , and  $\ddot{d}(t_n)$ , respectively. The equilibrium equations of discrete system under free vibration at times  $t_n$  and  $t_{n+1}$  are:

$$\begin{cases}
Ma_n + Kd_n = 0 \\
Ma_{n+1} + Kd_{n+1} = 0
\end{cases}$$
(48)

Taking the averages and differences of Eq. (48) directly yields:

$$\begin{cases}
M \left[ a_n \right] + K \left[ d_n \right] = 0 \\
M \left\langle a_n \right\rangle + K \left\langle d_n \right\rangle = 0
\end{cases}$$
(49)

where  $[\cdot] = (\cdot)_{n+1} - (\cdot)_n$  is the difference operator and  $\langle \cdot \rangle = \frac{1}{2} \left( (\cdot)_{n+1} + (\cdot)_n \right)$  is the average operator. Now recall the Newmark time integration algorithm for the displacements and velocities, cast in the predictor–corrector format:

$$\begin{cases} d_{n+1} = \tilde{d}_{n+1} + \beta \Delta t^2 a_{n+1} \\ v_{n+1} = \tilde{v}_{n+1} + \gamma \Delta t a_{n+1} \end{cases}$$
 (50)

where ( ) denotes the predicted quantities:

$$\begin{cases} \tilde{\boldsymbol{d}}_{n+1} = \boldsymbol{d}_n + \Delta t \boldsymbol{v}_n + \frac{1}{2} (1 - 2\beta) \Delta t^2 \boldsymbol{a}_n \\ \tilde{\boldsymbol{v}}_{n+1} = \boldsymbol{v}_n + (1 - \gamma) \Delta t \boldsymbol{a}_n \end{cases}$$
(51)

By substituting Newmark time integration in Eqs. (48)–(51), the change of total energy can be found as:

$$\left[ \bar{\boldsymbol{\Pi}} \right] = \frac{1}{2} \boldsymbol{v}_{n+1}^{\mathsf{T}} (\boldsymbol{M} - \boldsymbol{M}^{\mathsf{T}}) \boldsymbol{v}_n + \frac{1}{2} \boldsymbol{d}_n^{\mathsf{T}} (\boldsymbol{K} - \boldsymbol{K}^{\mathsf{T}}) \boldsymbol{d}_{n+1} + (\frac{1}{2} - \gamma) [\boldsymbol{d}_n]^{\mathsf{T}} \boldsymbol{K} [\boldsymbol{d}_n]$$

$$-\Delta t (\beta - \gamma/2) [\boldsymbol{a}_n]^{\mathsf{T}} \boldsymbol{M} [\boldsymbol{v}_n]$$

$$(52)$$

**Remark 9.** The terms  $\frac{1}{2}v_{n+1}^{\mathsf{T}}(M-M^{\mathsf{T}})v_n$  and  $\frac{1}{2}d_n^{\mathsf{T}}(K-K^{\mathsf{T}})d_{n+1}$  in Eq. (52) exist as a result of a non-symmetric system, which can be a potential issue and cause unbounded energy growth. Also, the explicit reproducing kernel collocation/finite-volume method is achieved when the lumped mass matrix is employed with  $\beta = 0$ .

**Remark 10.** It is well known that in traditional Newmark with Bubnov-Galerkin methods, it is possible to exactly conserve the energy with  $\beta = 1/4$  and  $\gamma = 1/2$ , which is the so-called average acceleration method. Here, from Eq. (52), one can see that this is no longer possible when a non-symmetric system is employed.

**Remark 11.** It is also well known that in traditional Newmark, there exists a class of unconditionally stable algorithms. Here, from Eq. (52), one can see that it is not possible to select parameters such that the energy will be bounded, and for non-symmetric systems, there are no unconditionally stable Newmark algorithms. Finally, as a corollary, it is quite possible that for non-symmetric systems, the solution may be unconditionally unstable (this will be revisited), at least if using the traditional Newmark method of fixed constants.

## 3.4. Stability analysis

Stability is arguably the most important aspect of any type of time integration algorithm. To perform the stability analysis of Newmark method, following the approach in [1], first premultiply M on both sides of Eqs. (50) and (51) to yield:

$$Md_{n+1} = Md_n + \Delta t M v_n + \frac{1}{2} \Delta t^2 \{ (1 - 2\beta) M a_n + 2\beta M a_{n+1} \}$$

$$Mv_{n+1} = Mv_n + \Delta t \{ (1 - \gamma) M a_n + \gamma M a_{n+1} \}$$
(53)

Then, to build connection of the field variables, one can eliminate  $a_{n+1}$  and  $a_n$  by using the free vibration equilibrium in Eq. (48):

$$Md_{n+1} = Md_n + \Delta t M v_n + \frac{1}{2} \Delta t^2 \{ (1 - 2\beta)(-Kd_n) + 2\beta(-Kd_{n+1}) \}$$

$$Mv_{n+1} = Mv_n + \Delta t \{ (1 - \gamma)(-Kd_n) + \gamma(-Kd_{n+1}) \}$$
(54)

Rearranging the terms in Eq. (54) and putting the above equations in matrix form immediately gives:

$$\begin{bmatrix} \mathbf{M} & \gamma \Delta t \mathbf{K} \\ \mathbf{0} & \mathbf{M} + \beta \Delta t^2 \mathbf{K} \end{bmatrix} \begin{Bmatrix} \mathbf{v}_{n+1} \\ \mathbf{d}_{n+1} \end{Bmatrix} = \begin{bmatrix} \mathbf{M} & -\Delta t (1 - \gamma) \mathbf{K} \\ \Delta t \mathbf{M} & \mathbf{M} - 1/2 \Delta t^2 (1 - 2\beta) \mathbf{K} \end{bmatrix} \begin{Bmatrix} \mathbf{v}_n \\ \mathbf{d}_n \end{Bmatrix}$$
(55)

Next, Eq. (55) can be simplified by employing the generalized eigenvalue analysis of stiffness and mass matrices with  $K\eta = (\omega^h)^2 M\eta$ , where  $(\omega^h)^2$  and  $\eta$  are the generalized eigenvalues and eigenmodes. Importantly, in this study, the eigenvalue  $(\omega^h)^2$  can be either a positive or negative value due to the non-symmetric feature of the matrices. Now, applying the modal decomposition to Eq. (55), for an arbitrary mode, one arrives at the following amplification matrix A:

$$\mathbf{A} = \begin{bmatrix} 1 & \gamma \Delta t \left(\omega^h\right)^2 \\ 0 & 1 + \beta \Delta t^2 \left(\omega^h\right)^2 \end{bmatrix}^{-1} \begin{bmatrix} 1 & -(1 - \gamma)\Delta t \left(\omega^h\right)^2 \\ \Delta t & 1 - (1 - 2\beta)\Delta t^2 / 2 \left(\omega^h\right)^2 \end{bmatrix}$$
(56)

Thus, the stability analysis of Newmark method gives the strict requirement on the spectral radius of A, denoted by  $\rho_A(A)$ , which can be summarized as:

$$\begin{cases} \rho_A(A) \le 1 & \text{No repeated eigenvalues} \\ \rho_A(A) < 1 & \text{Otherwise} \end{cases}$$
 (57)

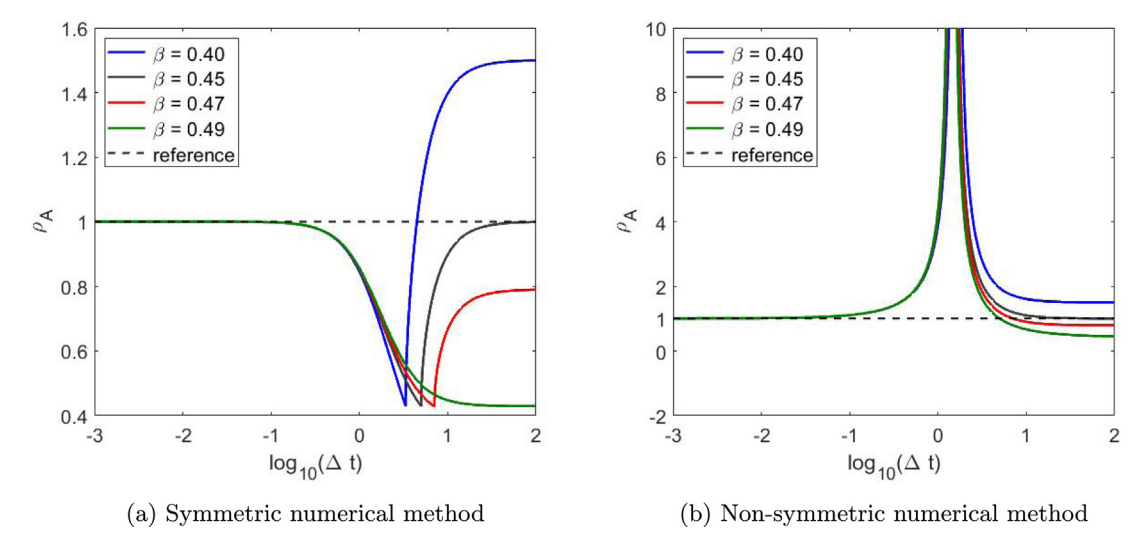


**Fig. 2.** Comparison of spectral radii with  $\gamma = 0.9$  varying  $\beta$ .

Since the spectral radius of a matrix is related to the norm of the maximum eigenvalue, one can first obtain the eigenvalues of the amplification matrix [1]:

$$\lambda_{1,2}(A) = A_1 \pm (A_1^2 - A_2)^{1/2} \tag{58}$$

where  $A_1 = \frac{1}{2} \operatorname{trace} A$  and  $A_2 = \det A$ . For Newmark method, one can show the following relationship for  $A_1$  and  $A_2$ :

$$A_{1} = 1 - \frac{\left(\omega^{h}\right)^{2} \Delta t^{2} (\gamma + 1/2)/2}{1 + \beta \left(\omega^{h}\right)^{2} \Delta t^{2}}$$

$$A_{2} = 1 - \frac{\left(\omega^{h}\right)^{2} \Delta t^{2} (\gamma - 1/2)}{1 + \beta \left(\omega^{h}\right)^{2} \Delta t^{2}}$$
(59)

For the non-symmetric method, one cannot preclude the possibility of  $(\omega^h)^2 < 0$ . For a very small time step  $\Delta t \ll 1$ , it is easy to show  $(A_1^2 - A_2)^{1/2} > 0$  and  $A_1 > 1$ . Subsequently, the following property of the spectral radius for the amplification matrix with respect to the negative eigenvalue is obtained:

$$\lim_{\Delta t \to 0} \rho_A(\mathbf{A}) = \lim_{\Delta t \to 0} \max \lambda_{1,2}(\mathbf{A}) = A_1 + \left(A_1^2 - A_2\right)^{1/2} > A_1 > 1 \tag{60}$$

which indicates that the spectral radius of the non-symmetric type amplification matrix is greater than unity when a very small time step is used, regardless of the choice of Newmark parameters.

A comparison of spectral radii is illustrated in Fig. 2. Here, the value of  $\gamma$  is fixed as 0.9, and the value of  $\beta$  is varied to see the behavior of spectral radii for the different time steps  $\Delta t$ . It can be noted that the main difference between a symmetric and non-symmetric method is the possible sign of  $(\omega^h)^2$ . Therefore, in Fig. 2(a), the value is manually set as  $(\omega^h)^2 = 1$  to represent a symmetric system. The value of  $(\omega^h)^2 = -1$  is prescribed to represent a non-symmetric system as shown Fig. 2(b). By conventional knowledge, when  $\gamma = 0.9$ , the cases corresponding to  $\beta \geq 0.45$  are unconditionally stable Newmark methods [1]. As given in Fig. 2(a), when  $\beta = 0.45$ ,  $\beta = 0.47$  and  $\beta = 0.49$ , the spectral radii are always below one, which indicates an unconditionally stable method. For the case with  $\beta = 0.40$ , the spectral radius is above one when the time step is large but will drop to a value below one after decreasing the time step, which is consistent with the conditionally stable requirement. However, using a non-symmetric system, because of the possible existence of a negative eigenvalue  $(\omega^h)^2$ , the spectral radii remains above one even when the time step is decreased as illustrated in Fig. 2(b): as the time step keeps decreasing it will not drop below one, which indicates that there is an *infimum* in this non-symmetric version. The stability in a non-symmetric method will not be guaranteed even as one decreases the time step. These results show that the

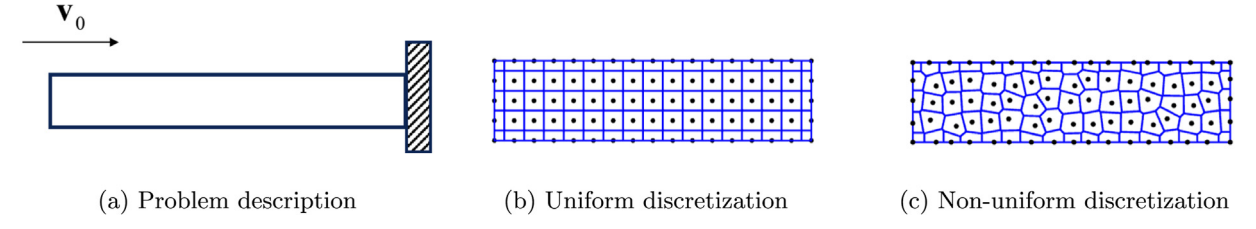


Fig. 3. Problem description of 2D wave propagation with 108 uniformly and non-uniformly distributed meshfree particles.

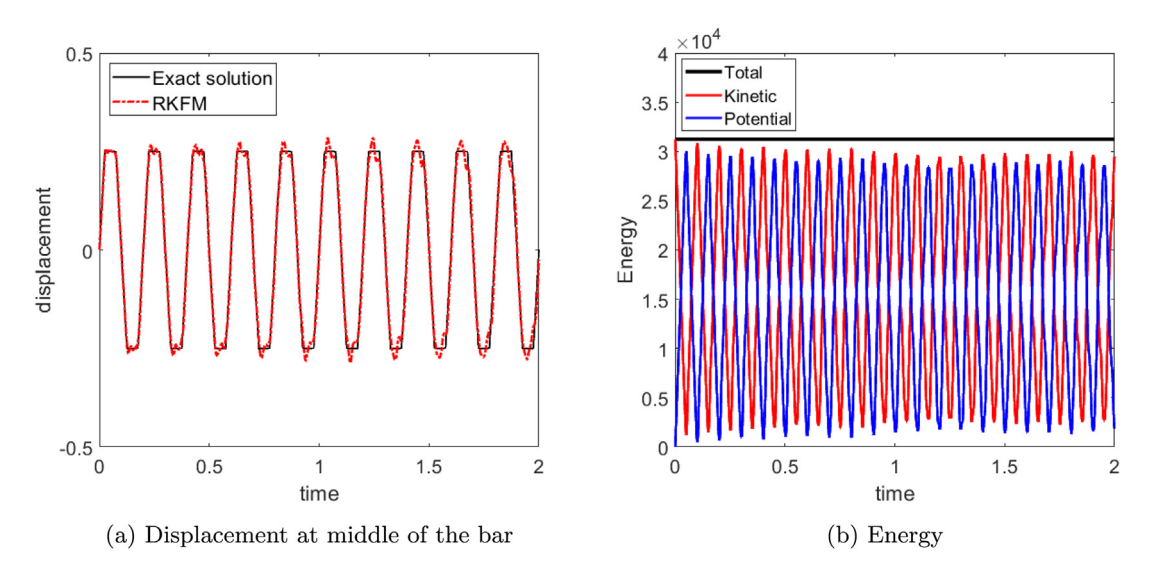


Fig. 4. Displacement at x = L/2 and energy results by solving momentum equation with uniform RKFM (quasi-symmetric matricies).

additional terms that result from employing non-symmetric systems in Eq. (52) will increase the energy of the system rather than dissipate it in the fully discrete case using Newmark.

#### 3.5. Demonstration of temporal instability in the Standard Newmark Method

To demonstrate the temporal instability due to the employment of non-symmetric system matrices, an elastic wave propagation problem is considered, with both uniform and non-uniform meshfree discretizations shown in Fig. 3. Standard Newmark time integration is used with the average acceleration scheme of  $\beta = 1/4$  and  $\gamma = 1/2$ , which by conventional knowledge exactly conserves the total energy of the system.

The reproducing kernel finite-volume method is employed in this subsection; the results for the collocation method will be formally presented in the numerical examples section. It is worth noting that under the uniform discretization, the reproducing kernel shape function exhibits a periodic and symmetric property, and thus the stiffness matrix constructed with RK shape functions is symmetric except the entries near the boundary, i.e.  $K \approx K^T$ . The RKFM simulation result under the uniform meshfree discretization is first given in Fig. 4. Using the quasi-symmetric stiffness matrix that results from using a uniform discretization, the displacement and energy results are similar to that of a Galerkin system: bounded with good accuracy in wave phase and amplitude. However, for the non-uniform discretization, the displacement and energy grows exponentially and finally yields a non-physical result, as shown in Fig. 5. Here the exact solution denotes the analytical solution with a very large number of terms in the series.

Next, a numerical experiment is performed: consider solving the energy conservation equation in Eq. (44) directly. This does not actually solve the governing equations of momentum conservation in the elastodynamic problem though (it should be obvious Eq. (41) is then violated for non-symmetric systems): the displacement history in

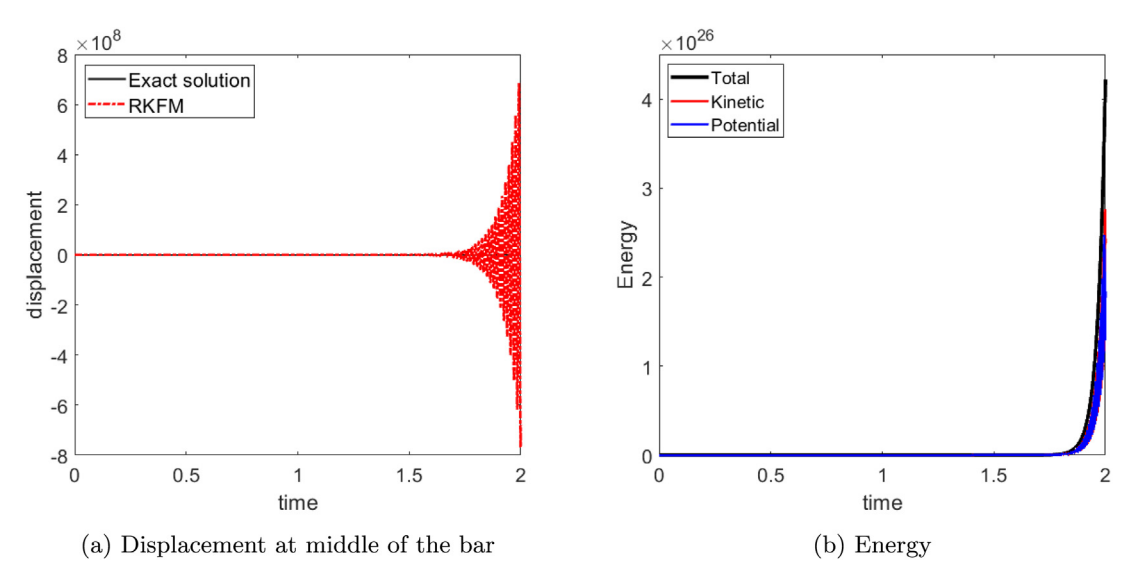


Fig. 5. Displacement at x = L/2 and energy results by solving momentum equation with non-uniform RKFM (non-symmetric matricies).

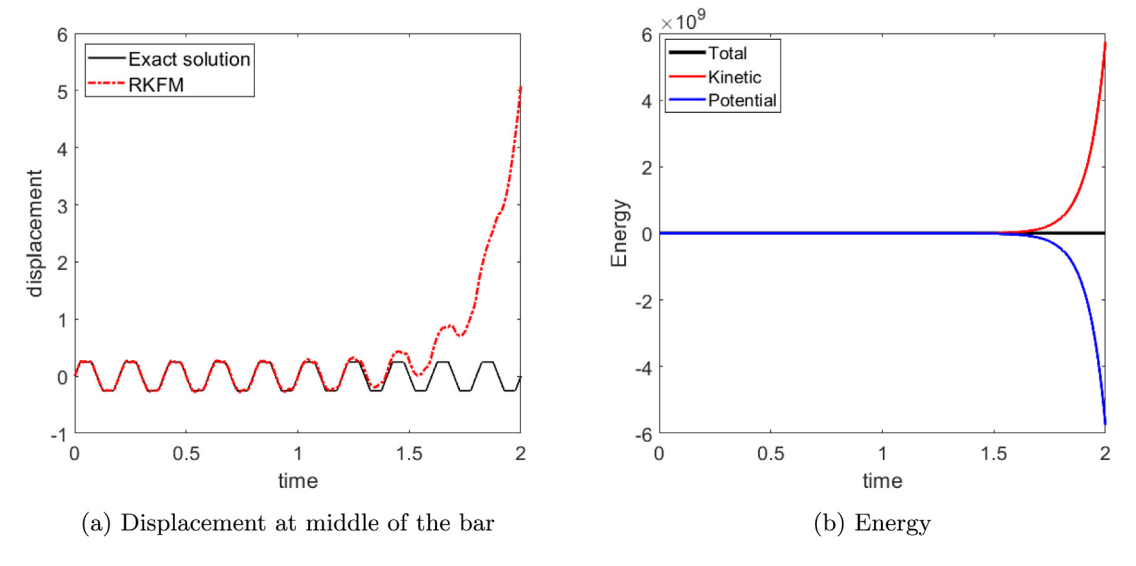


Fig. 6. Displacement at x = L/2 and energy results by solving energy equation with non-uniform RKFM (non-symmetric matricies).

Fig. 6(a) shows a spurious solution. In addition, while total energy is conserved as illustrated in Fig. 6(b), the kinetic and potential energy grow in an unbounded fashion. Thus, an energy conserving algorithm which also considers the momentum equation is needed for stabilizing elastodynamic problems when using non-symmetric systems.

## 4. Energy conservation algorithm for non-symmetric systems

Once the matrix system of equations is non-symmetric, the energy equation and momentum equation are not the same. Solving the momentum equation will fail to satisfy the energy equation, and vice versa. In this section, an energy conserving time integration algorithm is developed.

First, the conservation of semi-discrete energy requires the following relationship:

$$\dot{\Pi} = 0 \tag{61}$$

But considering discrete equilibrium, it is apparent that one cannot satisfy both (45a) and (45b) simultaneously in order to have both energy and linear momentum conserved, without requiring the symmetricity of the system matrices at hand.

Nevertheless, one can instead impose energy conservation in the fully discrete sense: first require the energy at state  $t = t_{n+1}$  be equal to the energy at state  $t = t_n$ :

$$\left[\bar{\Pi}\right] = 0\tag{62}$$

or

$$\bar{\Pi}_{n+1} = \bar{\Pi}_n \tag{63}$$

Using the definitions in Eq. (42), the following constraint is obtained:

$$\frac{1}{2} \mathbf{v}_{n+1}^{\mathsf{T}} \mathbf{M} \mathbf{v}_{n+1} - \frac{1}{2} \mathbf{v}_{n}^{\mathsf{T}} \mathbf{M} \mathbf{v}_{n} + \frac{1}{2} \mathbf{d}_{n+1}^{\mathsf{T}} \mathbf{K} \mathbf{d}_{n+1} - \frac{1}{2} \mathbf{d}_{n}^{\mathsf{T}} \mathbf{K} \mathbf{d}_{n} = (\mathbf{d}_{n+1} - \mathbf{d}_{n})^{\mathsf{T}} \mathbf{F}$$
(64)

where the force term is assumed to be a time independent variable, i.e.  $F_{n+1} = F_n = F$ . For general considerations with a time-dependent external force, the conservation law requires the following at the discrete level:

$$\dot{K}(\dot{\boldsymbol{u}}^h) + \dot{E}(\boldsymbol{u}^h) = \bar{P}(\dot{\boldsymbol{u}}^h) \tag{65}$$

The energy quantities at time  $t_{n+1}$  and  $t_n$  are obtained by integrating Eq. (65) on both sides, then one has:

$$K_{n+1} + E_{n+1} = \int_0^{t_{n+1}} \bar{P}(\dot{\boldsymbol{u}}^h) \, dt \tag{66}$$

$$K_n + E_n = \int_0^{t_n} \bar{P}(\dot{\boldsymbol{u}}^h) \, \mathrm{d}t \tag{67}$$

Therefore, the change of kinetic and potential energy is enforced to be equal to the work done by the power in the time slot  $[t_n, t_{n+1}]$ :

$$[K_n] + [E_n] = \int_{t_n}^{t_{n+1}} \bar{P}(\dot{\boldsymbol{u}}^h) dt$$
 (68)

where:

$$\int_{t_{n}}^{t_{n+1}} \bar{P}(\dot{\boldsymbol{u}}^{h}) dt = \int_{t_{n}}^{t_{n+1}} \left( \int_{\Omega} (\dot{\boldsymbol{u}}^{h}) \cdot \boldsymbol{b} d\Omega + \int_{\Gamma_{h}} (\dot{\boldsymbol{u}}^{h}) \cdot \bar{\boldsymbol{t}} d\Gamma \right) dt 
= \int_{\Omega} \dot{\boldsymbol{u}}_{n+\alpha}^{h} \cdot \int_{t_{n}}^{t_{n+1}} \boldsymbol{b} dt d\Omega + \int_{\Gamma_{h}} \dot{\boldsymbol{u}}_{n+\alpha}^{h} \cdot \int_{t_{n}}^{t_{n+1}} \bar{\boldsymbol{t}} dt d\Gamma 
\approx \int_{\Omega} \frac{\boldsymbol{u}_{n+1}^{h} - \boldsymbol{u}_{n}^{h}}{\Delta t} \cdot \frac{\Delta t}{2} (\boldsymbol{b}_{n+1} + \boldsymbol{b}_{n}) d\Omega 
+ \int_{\Gamma_{h}} \frac{\boldsymbol{u}_{n+1}^{h} - \boldsymbol{u}_{n}^{h}}{\Delta t} \cdot \frac{\Delta t}{2} (\bar{\boldsymbol{t}}_{n+1} + \bar{\boldsymbol{t}}_{n}) d\Gamma 
= \frac{1}{2} (\boldsymbol{d}_{n+1} - \boldsymbol{d}_{n})^{\mathsf{T}} (\boldsymbol{F}_{n+1} + \boldsymbol{F}_{n})$$
(69)

where the generalized  $\alpha$  trapezoidal rule is employed to calculate the external work term. It can be noted that when the force term is time independent, Eq. (68) immediately recovers Eq. (64). With the energy conservation equations in hand, the algorithm can now be defined.

First, the equilibrium equation at any time step  $t_{n+1}$  is strictly adhered to:

$$Ma_{n+1} + Kd_{n+1} = F_{n+1}.$$
 (70)

The displacement is advanced in time, as in the Newmark time integration algorithm:

$$\boldsymbol{d}_{n+1} = \tilde{\boldsymbol{d}}_{n+1} + \beta \Delta t^2 \boldsymbol{a}_{n+1} \tag{71}$$

where

$$\tilde{\boldsymbol{d}}_{n+1} = \boldsymbol{d}_n + \Delta t \boldsymbol{v}_n + \frac{1}{2} (1 - 2\beta) \Delta t^2 \boldsymbol{a}_n. \tag{72}$$

Combining Eqs. (70) and (71), the acceleration at  $t_{n+1}$  is found from:

$$(\mathbf{M} + \beta \Delta t^2 \mathbf{K}) \mathbf{a}_{n+1} = \mathbf{F}_{n+1} - \mathbf{K} \tilde{\mathbf{d}}_{n+1} \tag{73}$$

The final displacement is then found from the corrector (71). The discrete energy conservation constraint is then employed to solve for the velocities:

$$\frac{1}{2} \mathbf{v}_{n+1}^{\mathsf{T}} \mathbf{M} \mathbf{v}_{n+1} - \frac{1}{2} \mathbf{v}_{n}^{\mathsf{T}} \mathbf{M} \mathbf{v}_{n} + \frac{1}{2} \mathbf{d}_{n+1}^{\mathsf{T}} \mathbf{K} \mathbf{d}_{n+1} - \frac{1}{2} \mathbf{d}_{n}^{\mathsf{T}} \mathbf{K} \mathbf{d}_{n}$$

$$= \frac{1}{2} (\mathbf{d}_{n+1} - \mathbf{d}_{n})^{\mathsf{T}} (\mathbf{F}_{n+1} + \mathbf{F}_{n})$$

$$= [\mathbf{d}_{n}]^{\mathsf{T}} \langle \mathbf{F}_{n} \rangle$$
(74)

As can be seen, both the momentum equation (70) as well as the conservation of energy (63) are satisfied in the proposed algorithm for the fully discrete system. Interestingly, as we have shown, this does not appear to be possible in the semi-discrete case.

In contrast to the solution procedure of traditional Newmark time integration algorithm, the velocity is calculated with Eq. (74) instead of using the definitions of velocity in Eqs. (50) and (51).

However, the velocities  $v_{n+1}$  represent multiple unknowns, but the condition provided for solving velocities so far is only the energy equation in Eq. (74), which represents a scalar relationship. To reduce the multiple degree of freedom system to a single equation, a variable time integration controlling parameter  $\tilde{\gamma}$  is introduced:

$$\mathbf{v}_{n+1} = \mathbf{v}_n + \Delta t \mathbf{a}_n + \Delta t \tilde{\gamma} (\mathbf{a}_{n+1} - \mathbf{a}_n) \tag{75}$$

Substituting Eq. (75) into Eq. (74), using the fact that  $a_{n+1}$  and  $d_{n+1}$  are known from Eqs. (73) and (71), the condition in Eq. (74) reduces to:

$$f(\tilde{\gamma}) = a\tilde{\gamma}^2 + b\tilde{\gamma} + c = 0 \tag{76}$$

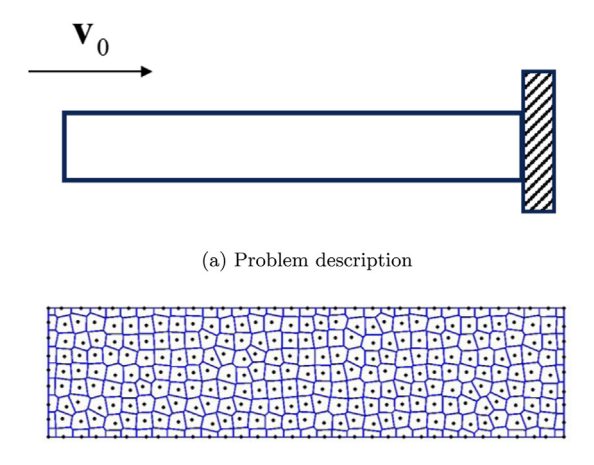
where:

$$\begin{cases}
a = \frac{1}{2} \Delta t^{2} [\boldsymbol{a}_{n}]^{\mathsf{T}} \boldsymbol{M} [\boldsymbol{a}_{n}] \\
b = \Delta t [\boldsymbol{v}_{n} + \Delta t \boldsymbol{a}_{n}]^{\mathsf{T}} \boldsymbol{M} [\boldsymbol{a}_{n}] \\
c = -\frac{1}{2} \boldsymbol{v}_{n}^{\mathsf{T}} \boldsymbol{M} \boldsymbol{v}_{n} - \frac{1}{2} \boldsymbol{d}_{n}^{\mathsf{T}} \boldsymbol{K} \boldsymbol{d}_{n} + \frac{1}{2} \boldsymbol{d}_{n+1}^{\mathsf{T}} \boldsymbol{K} \boldsymbol{d}_{n+1} \\
-[\boldsymbol{d}_{n}]^{\mathsf{T}} \langle \boldsymbol{F}_{n} \rangle + \frac{1}{2} [\boldsymbol{v}_{n} + \Delta t \boldsymbol{a}_{n}]^{\mathsf{T}} \boldsymbol{M} [\boldsymbol{v}_{n} + \Delta t \boldsymbol{a}_{n}]
\end{cases} \tag{77}$$

The coefficients in Eq. (76) can be computed at the current time step  $t_{n+1}$ . After the calculation of  $\tilde{\gamma}$  in Eq. (76), the velocity vector is updated by Eq. (75), which provides enforcement of the discrete conservation of total energy by adjusting the velocities.

**Remark 12.** The energy control algorithm can also be viewed as an adaptive type of Newmark time integration. In other words, this method seeks the proper value of  $\tilde{\gamma}$  in each time step from Eq. (76). The overall philosophy is to introduce a proper numerical dissipation with  $\gamma > 1/2$ , such that the energy is conserved since the non-symmetric systems tend to provide a negative dissipation, or energy growth. Therefore, the total change of energy from time  $t_n$  to  $t_{n+1}$  is exactly zero when an appropriate  $\tilde{\gamma}$  is utilized for Newmark time integration. Compared to the standard Newmark approach, an updated  $\tilde{\gamma}$  replaces a constant  $\gamma$  in the traditional method, which brings forth the idea that the Newmark parameters can be considered as a variable as well.

Remark 13. The energy conserving algorithm is fulfilled by obtaining  $\tilde{\gamma}$  from Eq. (76) where no difficulty in obtaining roots has been encountered for the examples here. However, in more complex situations, such as when inelasticity is present, the authors have found that sometimes imaginary roots can be obtained. The generalization of the present algorithm (or a necessary modification) to the case of finite-strain and/or inelasticity needs closer examination and should be considered in future work. Overall, it can be seen that a key feature to consider in any future energy conservation algorithms is the quadratic nature of the energy-type terms which seems difficult to avoid.



(b) Uniform discretization with 297 particles

Fig. 7. Problem description of 2D wave propagation with non-uniform meshfree discretization.

#### 5. Numerical examples

In this section, several 2D numerical examples under non-uniform meshfree collocation and finite-volume discretizations (which yield non-symmetric matrices) are provided to verify the effectiveness of proposed method. Meanwhile, the lumped mass matrices are employed.

## 5.1. 2D Non-uniform wave propagation in elastic media

The first numerical example considered is a 2D bar with a fixed end, as shown in Fig. 7. The dimensions of the bar are length L in the x-direction, and height H in the y-direction, with the origin on the bottom left. The whole bar is subjected to an initial velocity  $v_0 = 10 \text{ m/s}$  in the x-direction. The material properties are: density  $\rho = 100 \text{ kg/m}^3$ , Young's modulus  $E = 10^6 \text{ Pa}$  and Poisson's ratio v = 0.0 The analytical is given as a 1D relationship, however in this problem it will be modeled as 2D (with Poisson's ratio v = 0.0). Free boundaries are set on x = 0, y = 0 and y = H. The fixed essential boundary is on x = L. The corresponding analytical solution for the 2D wave propagation problem is as follows:

$$u_x(\mathbf{x},t) = \sum_{n=1}^{\infty} A_n \sin(w_n t) \cos[(2n-1)\frac{\pi x}{2L}]$$

$$u_y(\mathbf{x},t) = 0$$
(78)

where:

$$A_{n} = \frac{8Lv_{0}(-1)^{n+1}}{[(2n-1)\pi]^{2}c}$$

$$w_{n} = \frac{(2n-1)\pi c}{2L}$$

$$c = \sqrt{E/\rho}$$
(79)

The problem is simulated using both the reproducing kernel collocation and reproducing kernel finite-volume methods with the nonuniform meshfree discretization shown in Fig. 7(b). A normalized support size of 2.3 with a quadratic basis function is employed in RKCM, since the minimum requirement for convergent solutions in the collocation method is quadratic accuracy [12]. On the other hand, since only the first order derivatives are needed in the reproducing kernel finite-volume formulation, linear basis is enough to guarantee convergence in space; therefore linear basis with a normalized support size of 1.3 is employed. The time step is set as  $\Delta t = 0.0001$  for both RCKM and RKFM, and the explicit central difference algorithm is employed ( $\beta = 0$  and  $\gamma = 1/2$ ). The time step is well below the conventional critical time step based on the problem constants and grid spacing.

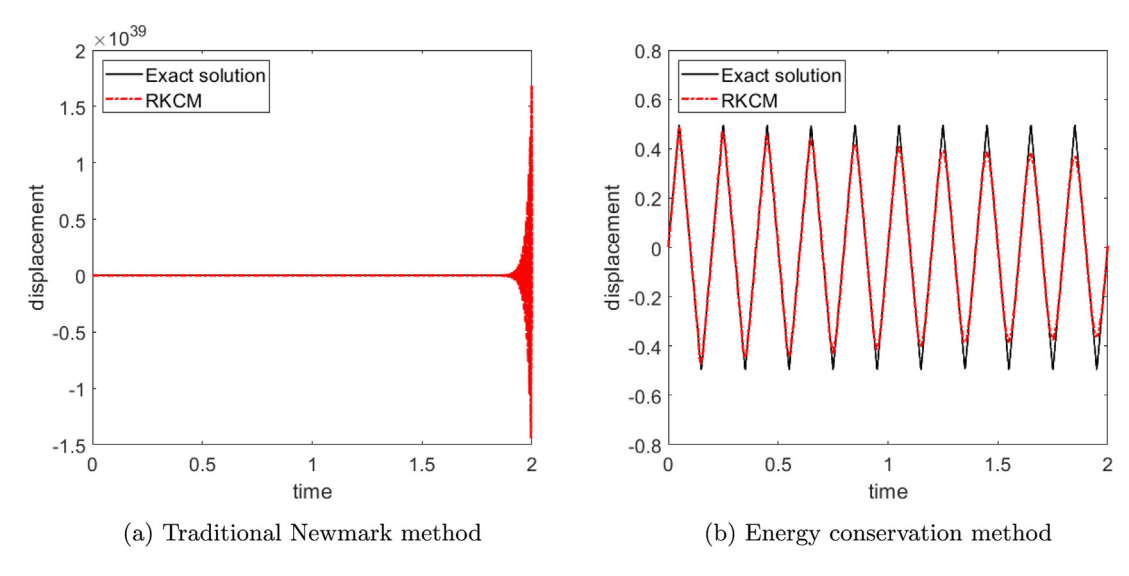


Fig. 8. Displacement results at x = 0 with non-uniform reproducing kernel collocation method (RKCM).

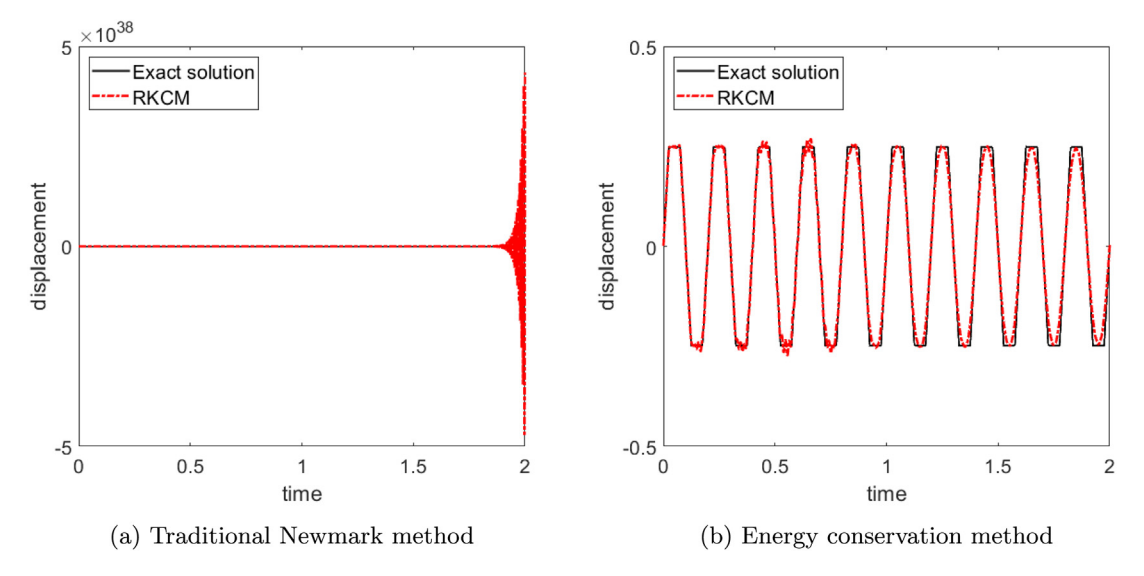


Fig. 9. Displacement results at x = L/2 with non-uniform reproducing kernel collocation method (RKCM).

The displacement time histories of RKCM for two locations on the bar are shown in Figs. 8 and 9. As can be seen from Figs. 8(a) and 9(a), the use of the traditional Newmark time integration algorithm will eventually yield unbounded results. This result confirms the analyses provided that shows the Newmark algorithm will in general, yield exponential growth when employing non-symmetric system matrices. On the other hand, by employing the proposed energy conservation algorithm, the results agree well with the analytical solution as shown in Figs. 8(b) and 9(b). The plots of the kinetic, potential, and total energy are provided in Fig. 10 for the collocation method. Unbounded energy growth is observed when the traditional Newmark method is used. This issue can be resolved by employing the energy conservation algorithm as shown in Fig. 10(b). Since the system does not contain any external forces, the total energy should be a constant value. Here it can be seen that the proposed algorithm exactly conserves the total numerical energy of the system.

The displacement histories using the reproducing kernel finite-volume method are provided in Figs. 11 and 12, which give direct comparisons between the traditional Newmark algorithm and the proposed energy conservation

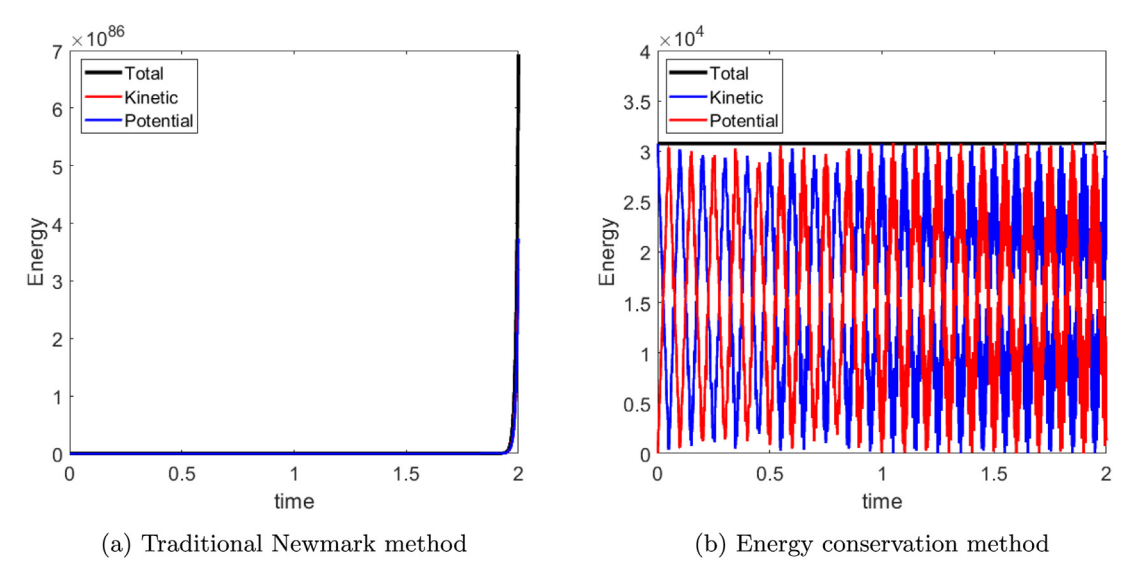


Fig. 10. Energy results with non-uniform reproducing kernel collocation method (RKCM).

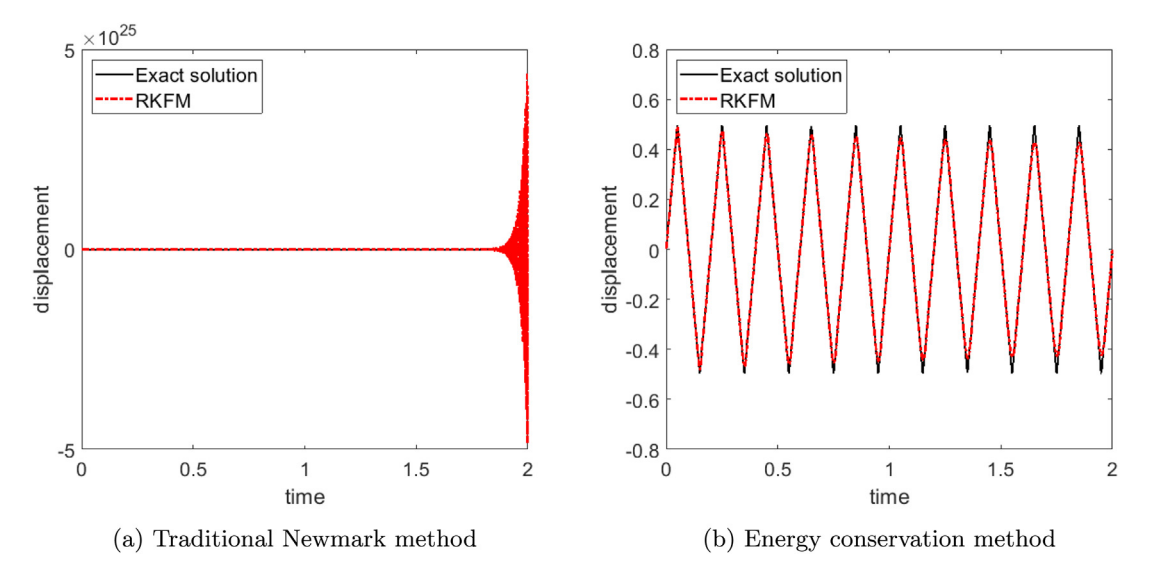


Fig. 11. Displacement results at x = 0 with non-uniform reproducing kernel finite-volume method (RKFM).

algorithm. Similar to the collocation method, and previous examples, the traditional Newmark method provides unbounded solutions, while the energy conserving algorithm stays bounded and also agrees well with the analytical solutions. The comparison of system energies is shown in Fig. 13; the energy of the Newmark method for the non-symmetric system grows exponentially, while the proposed algorithm exactly conserves the total energy of the discrete system.

In summary, unbounded numerical results have been observed when non-symmetric numerical methods are employed, which can be addressed by the proposed algorithm. Interestingly, with this algorithm, the energy can also be exactly conserved even when using an explicit solution strategy ( $\beta=0$ ), which is not feasible in the traditional Newmark time integration algorithm. The key feature of the current implementation of the method is that the velocity update parameter  $\bar{\gamma}$  is no longer a constant value. The history of  $\bar{\gamma}$  provided in Fig. 14 demonstrates how the parameter varies in time to control the energy. Here it is seen that the RKFM solution exhibits a comparatively steady state when compared to RKCM.

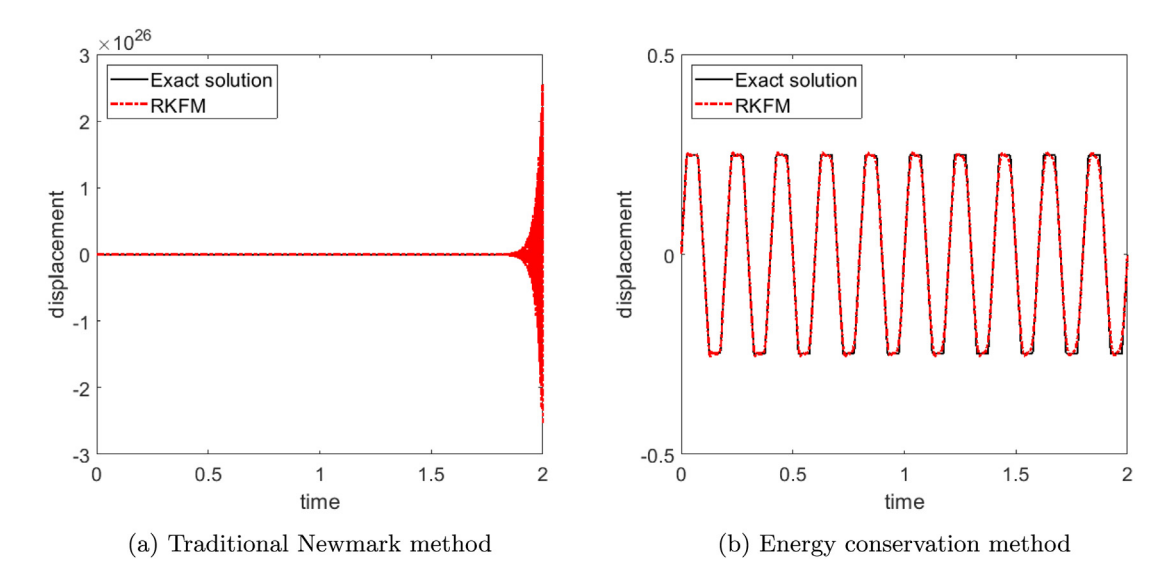


Fig. 12. Displacement results at x = L/2 with non-uniform reproducing kernel finite-volume method (RKFM).

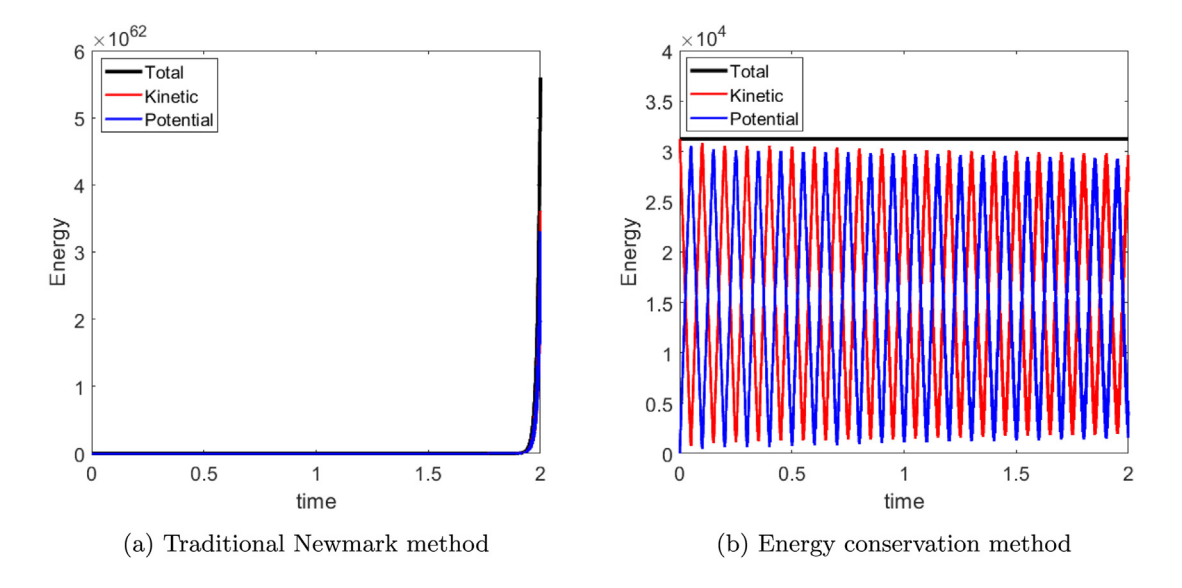


Fig. 13. Energy results with non-uniform reproducing kernel finite-volume method (RKFM).

## 5.2. 2D Elasticity problem with periodic loading

The next numerical example considered is the 2D bar shown in Fig. 15(a), which has the same geometry as the previous test. In contrast to the previous wave propagation problem, the bar is subjected to a periodic traction  $F = EA\sin(\bar{\omega}t)$  along the x-direction at the end of the bar, where  $\bar{\omega}$  denotes the frequency and A is the amplitude. This problem aims to examine the effectiveness of the energy conservation algorithm in the general case of systems with external forces. Under the external load, the sum of the kinetic and potential energy is no longer constant, and the rate of change in the physical system is equal to the external power, rather than zero. The strong form of the

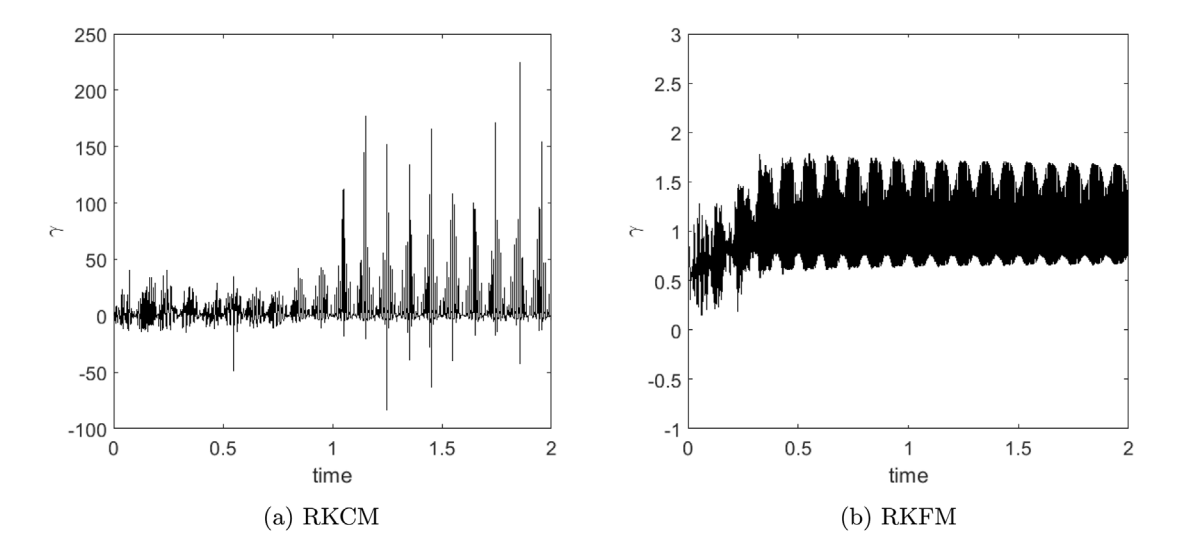


Fig. 14. Comparison between RKCM and RKFM for history of  $\bar{\gamma}$  with energy conservation algorithm.

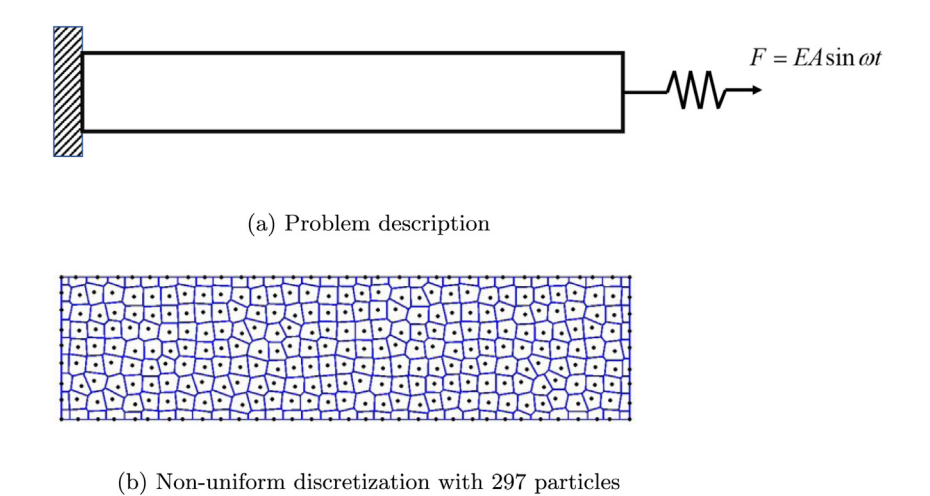


Fig. 15. Problem description of 2D bar under periodic loading with non-uniform meshfree discretization.

problem is:

$$\begin{cases}
\rho \ddot{\boldsymbol{u}} - \nabla \cdot \boldsymbol{\sigma} = \boldsymbol{0} & \text{in } \Omega \\
\boldsymbol{u}(\boldsymbol{x}, t) = \boldsymbol{0} & \text{on } \boldsymbol{x} = 0 \\
\boldsymbol{\sigma} \cdot \boldsymbol{n} = \{EA \sin \bar{\omega}t, 0\}^{\mathsf{T}} & \text{on } \boldsymbol{x} = L \\
\boldsymbol{\sigma} \cdot \boldsymbol{n} = \boldsymbol{0} & \text{on } \boldsymbol{y} = H \\
\boldsymbol{\sigma} \cdot \boldsymbol{n} = \boldsymbol{0} & \text{on } \boldsymbol{y} = 0
\end{cases}$$
(80)

with the initial conditions:

$$\begin{cases} \mathbf{u}(x,0) = \mathbf{0} \\ \dot{\mathbf{u}}(x,0) = \mathbf{0} \end{cases}$$
(81)

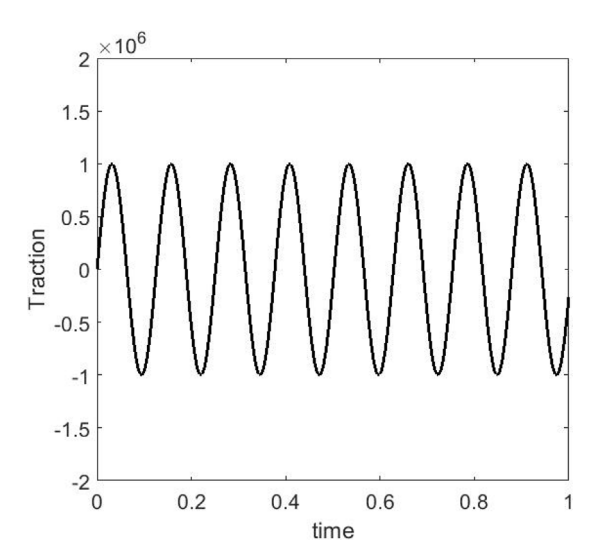


Fig. 16. The periodic loading history.

The analytical solution corresponding to Eq. (80) is:

$$u_x = \sin(\bar{\omega}t)p(\mathbf{x}) - \sum_{n=1}^{\infty} \frac{4\bar{\omega}q_n}{(2n-1)\pi c} \sin\left(\frac{2n-1}{2L}\pi ct\right) \sin\left(\frac{2n-1}{2L}\pi x\right)$$
(82)

 $u_y = 0$ 

where:

$$q_n = \int_0^L p(\mathbf{x}) \sin\left(\frac{2n-1}{2L}\pi x\right) dx \tag{83}$$

$$p(\mathbf{x}) = \frac{Ac}{\bar{\omega}\cos(\bar{\omega}L/c)}\sin(\bar{\omega}x/c) \tag{84}$$

The material properties for this problem are: density  $\rho=100~{\rm kg/m^3}$ , Young's modulus  $E=10^6$  Pa and Poisson's ratio v=0.0. The loading frequency and amplitude are set as  $\bar{\omega}=50$  and A=1, respectively. The traction loading history is plotted in Fig. 16. For RKCM and RKFM, the RK parameters in the previous example are employed. The displacement histories are provided in Figs. 17 and 18 for RKCM. The associated results for the energy are shown in Fig. 19. It can be seen that without the energy conservation algorithm, the displacement and energy grow exponentially as before. Since an external force is involved here, the total energy (sum of the kinetic and potential energy) will not be a constant value, but it nevertheless remains bounded when using the proposed algorithm.

For RKFM, similar results shown in Figs. 20–22 have been obtained. However, the amplitude of traditional Newmark results are much lower than the one with RKCM. Meanwhile, the comparison of the history of  $\bar{\gamma}$  in Fig. 23 shows similar features as the last example: the range of  $\bar{\gamma}$  in the RKFM simulation is relatively small compared to RKCM, and is much closer to the traditional value of 1/2. In other words, the RKFM method is more stable compared to RKCM.

## 5.3. Split-Hopkinson Bar

As a comprehensive study of the effectiveness of proposed method, a test of a split Hopkinson bar shown in Fig. 24 is presented. The model is generated from a micro-computed-tomography (micro-CT) scan, and this problem features highly irregular geometry. The material is considered as elastic with density  $\rho = 2160 \text{ kg/m}^3$ , Young's modulus E = 31GPa and Poisson's ratio v = 0.2. A traction load from an experiment is applied in the x -direction, with time history shown in Fig. 24(b). Stress distributions given by RKFM modeling for the standard Newmark and energy conservation methods at 60  $\mu$ s and 240  $\mu$ s are presented in Figs. 25 and 26. The stress results of these two

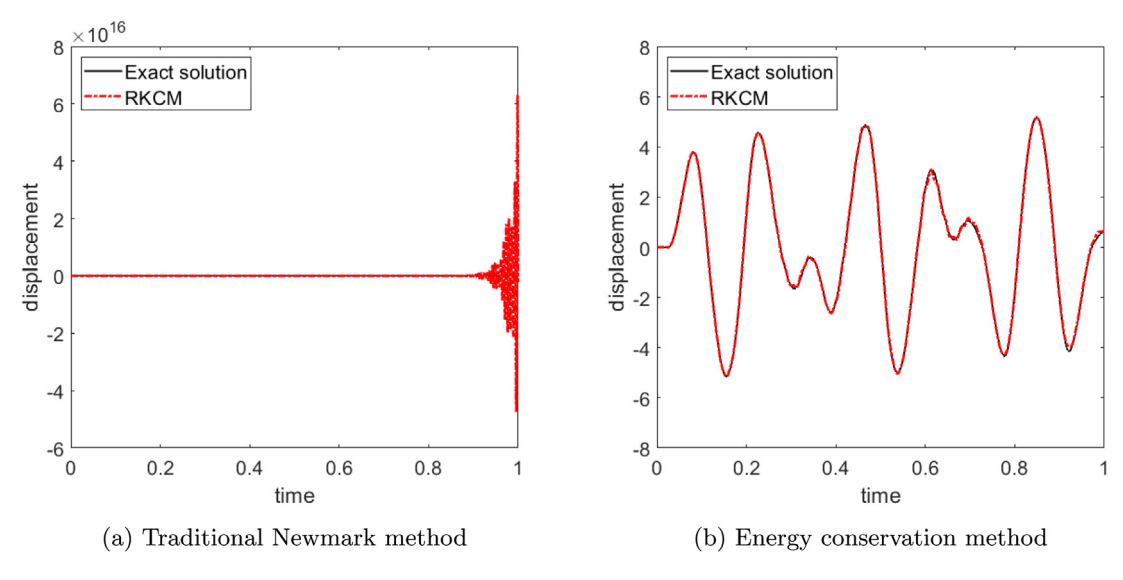


Fig. 17. Displacement results at x = L/2 with non-uniform reproducing kernel collocation method (RKCM).

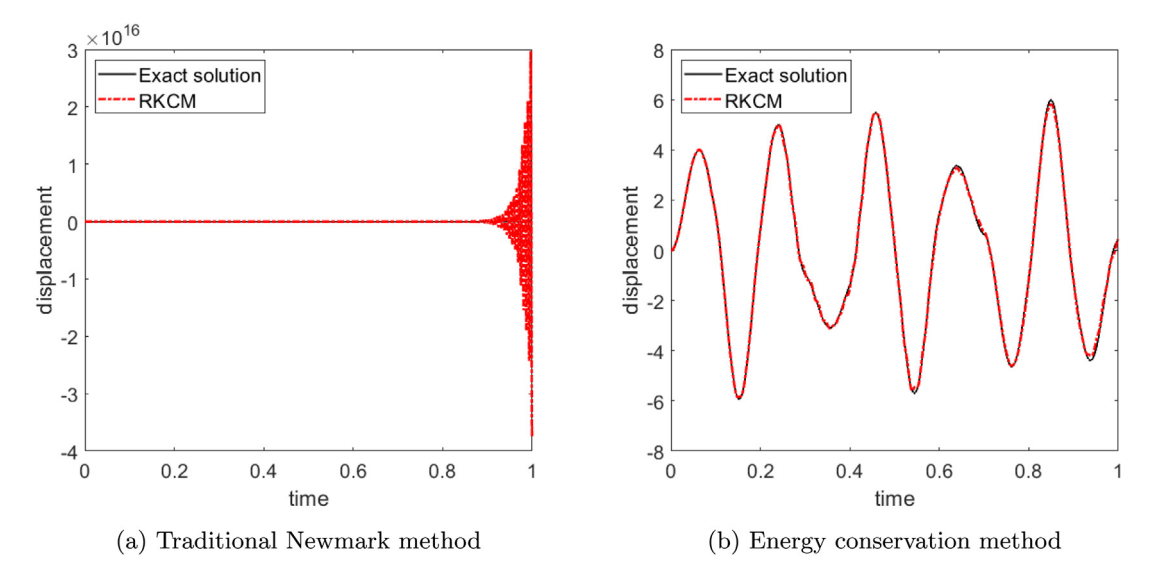


Fig. 18. Displacement results at x = L with non-uniform reproducing kernel collocation method (RKCM).

methods at 60 µs are comparable, but become highly oscillatory at 240 µs for standard Newmark, while a stable result can be found from the energy controlled method in Fig. 26(b).

#### 6. Conclusions

An energy conserving time integration algorithm has been developed to control the possible unbounded energy growth when using non-symmetric systems in the solution of elastodynamics. It has been systematically shown that the conservation of linear momentum and energy are equivalent in the continuous sense, but only conditionally equivalent in the semi-discrete sense: the symmetry of the mass and stiffness matrices is necessary. Thus when employing a Bubnov-Galerkin method, solving the momentum equation solves the energy equation. However, when using non-symmetric methods, as in the classes of collocation, Petrov–Galerkin, and finite volume methods, solving the momentum equation violates the energy equation, and vice versa.

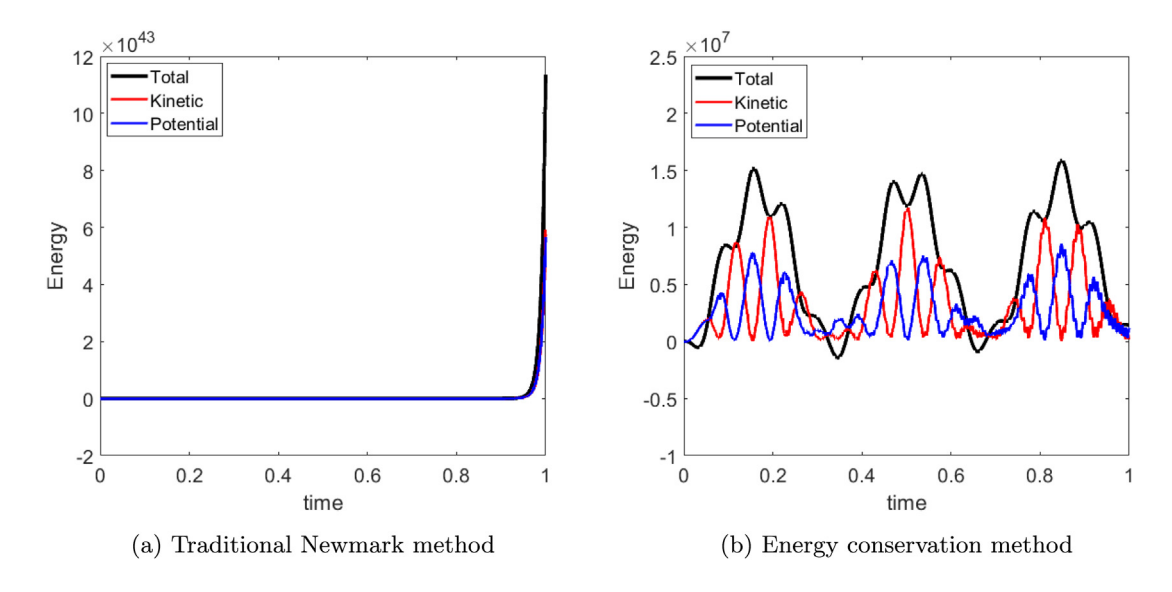


Fig. 19. Energy results with non-uniform reproducing kernel collocation method (RKCM).

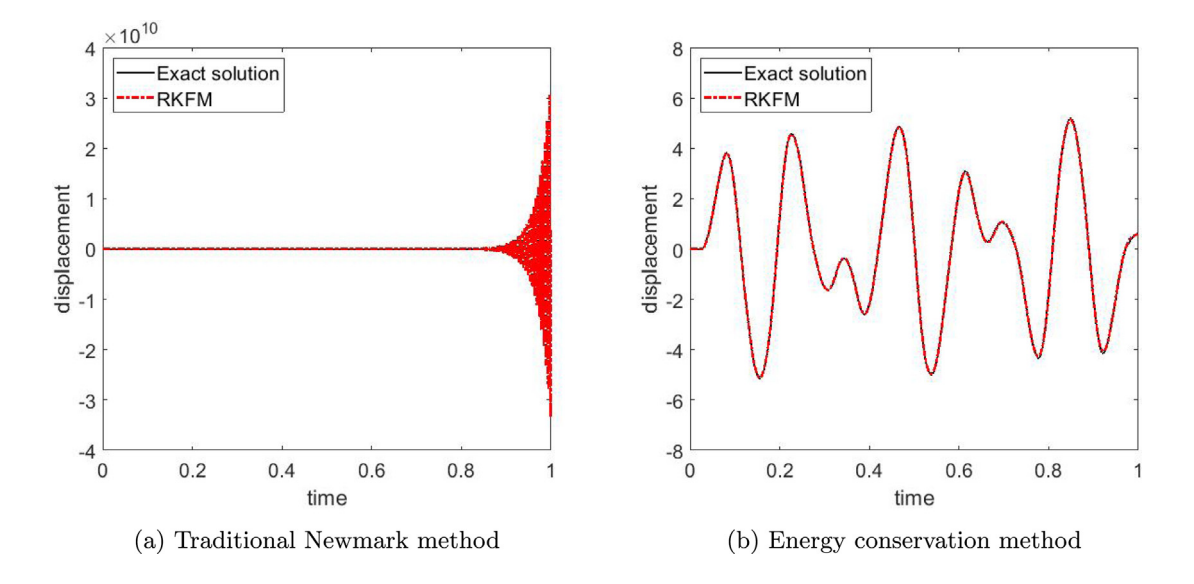


Fig. 20. Displacement results at x = L/2 with non-uniform reproducing kernel finite-volume method (RKFM).

The temporal numerical stability of the full discretization of elastodynamic problems for non-symmetric systems was also analyzed. The spectral radius of the amplification matrix shows that unconditionally unstable behavior is possible due to the existence of a negative generalized eigenvalue. Therefore, the critical condition for the temporal stability is the existence of all positive eigenvalues, which can be assured by employing symmetric matrices with sufficient stability, but cannot necessarily be guaranteed for non-symmetric systems. An energy control algorithm was established for elastodynamic problems, which includes the equation of motion, time integration on displacement, and velocities calculated from the energy equation. Stable results have been observed in the numerical examples. The wave propagation problem and bar under periodic loading showed good agreement with the analytical solutions when using the energy conservation method, but unbounded results with the standard Newmark method.

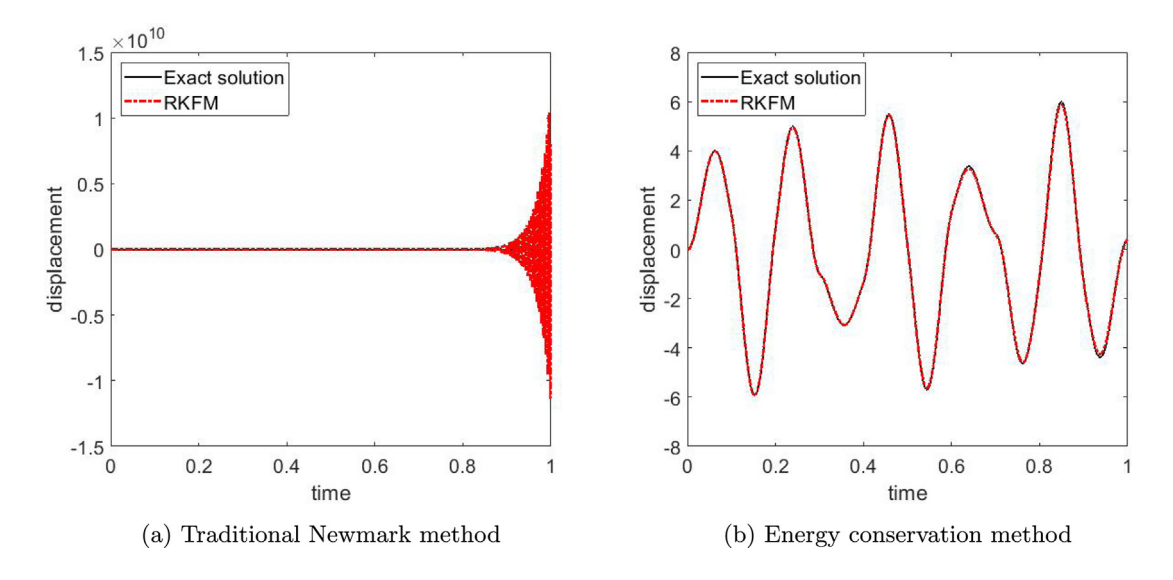


Fig. 21. Displacement results at x = L with non-uniform reproducing kernel finite-volume method (RKFM).

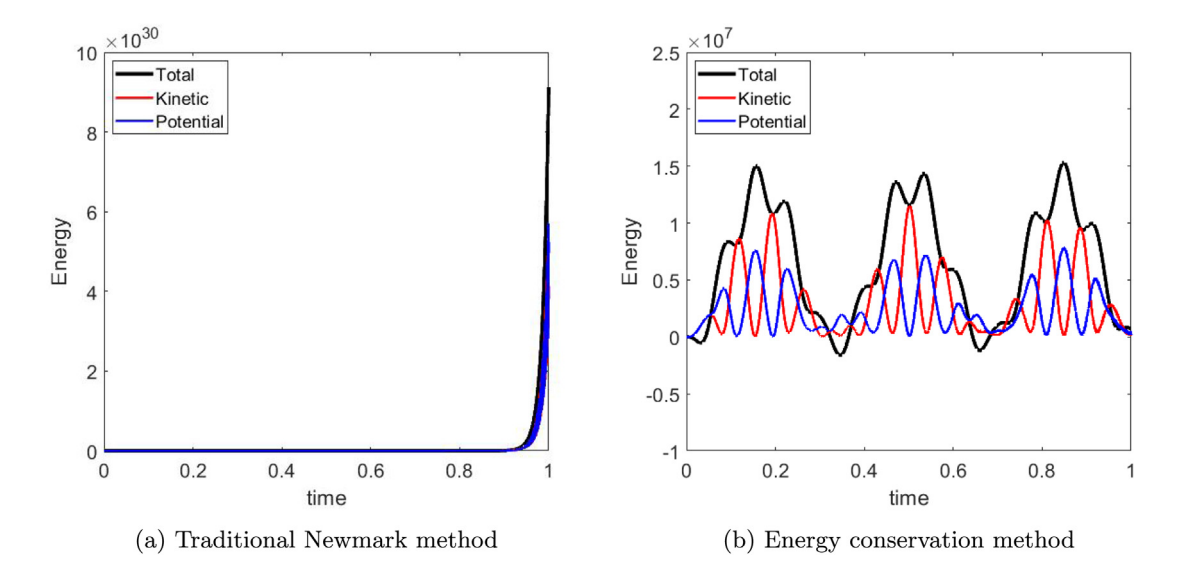


Fig. 22. Energy results with non-uniform reproducing kernel finite-volume method (RKFM).

The CT-scan problem with complex geometry was further used to verify the robustness of proposed method. The instability in non-symmetric systems when using traditional methods, and the effectiveness of the energy conservation time integration algorithm, have both been successfully demonstrated.

The specific solution algorithm tested is based on varying a velocity time integration parameter in order to satisfy the energy equation, although this is only one way to implement the method and satisfy the scalar condition. Many other possibilities likely exist, which may be more robust than the current strategy, which results in a quadratic equation which could become problematic depending on the roots. In more complex situations such as inelasticity, we have found that imaginary roots can be obtained, or no roots at all. The general case of finite-strain and/or inelasticity needs closer examination and should be considered in future work.

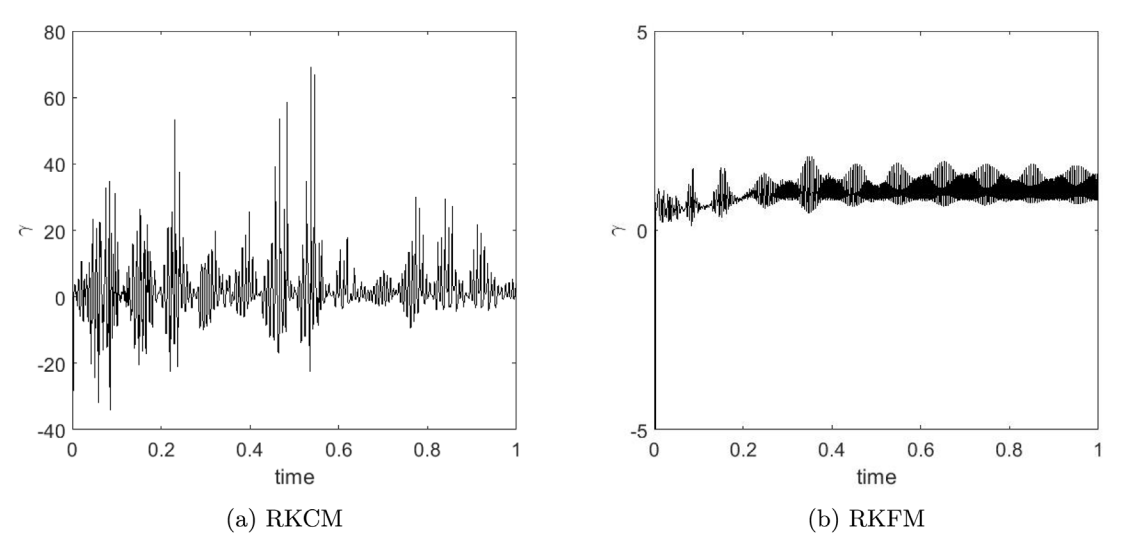


Fig. 23. Comparison between RKCM and RKFM for history of  $\bar{\gamma}$  with energy conservation algorithm.

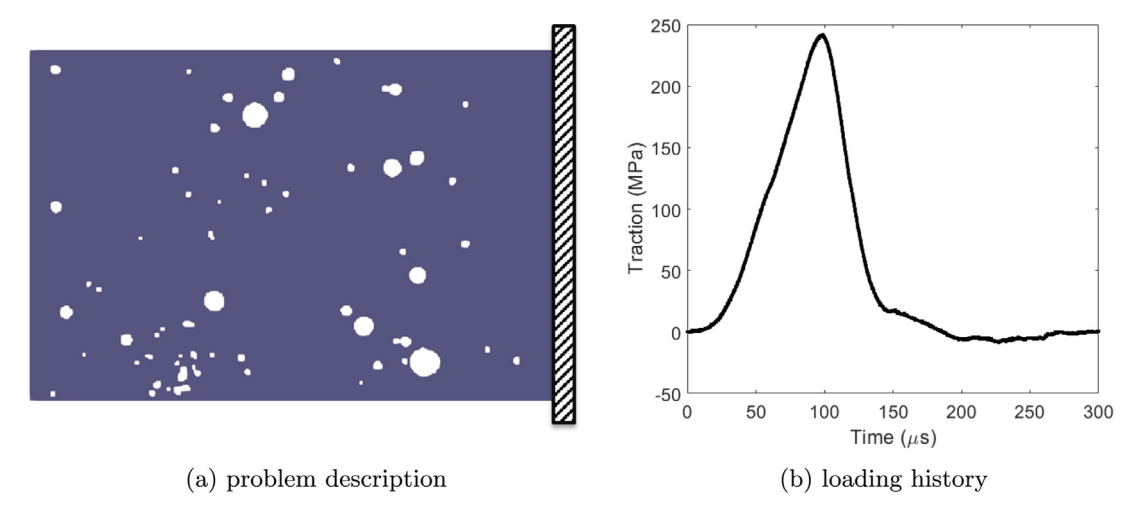


Fig. 24. Problem description of split-Hopkinson bar specimen after CT scan.

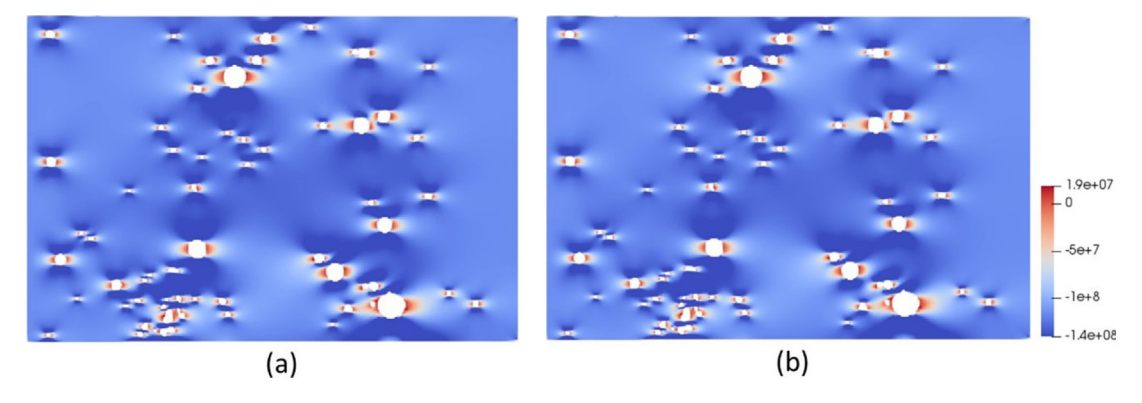


Fig. 25. Comparison of  $\sigma_{xx}$  at 60  $\mu s$  (a) standard Newmark method; (b) energy conservation method.

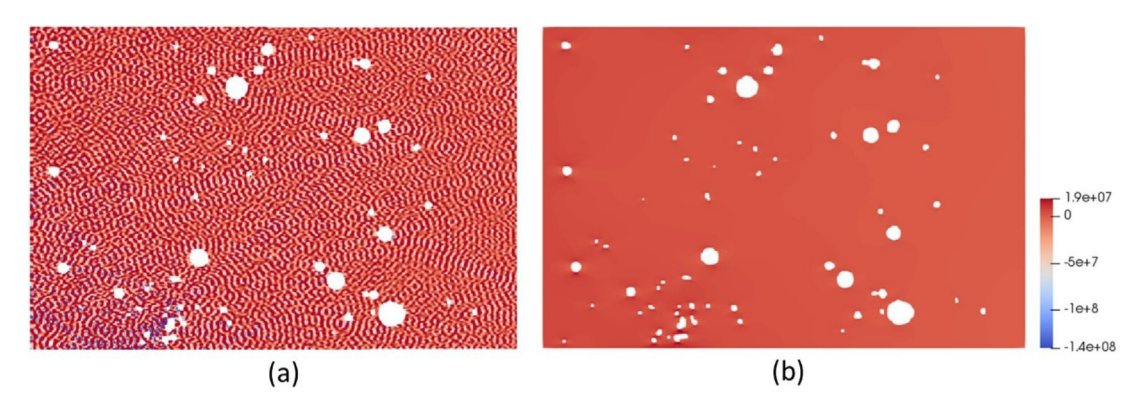


Fig. 26. Comparison of  $\sigma_{xx}$  at 240 µs: (a) standard Newmark method; (b) energy conservation method.

## **Declaration of competing interest**

The authors declare that they have no known competing financial interests or personal relationships that could have appeared to influence the work reported in this paper.

## Acknowledgments

This work was supported by the National Science Foundation, USA award number 1826221 and the U.S. Army Engineering Research and Development Center through Ordnance Technology Initiative Agreement, USA DOTC-17-01-INIT0880. Proofing of this manuscript by Jennifer Dougal is also acknowledged and appreciated.

#### References

- [1] T.J. Hughes, The Finite Element Method: Linear Static and Dynamic Finite Element Analysis, Courier Corporation, 2012.
- [2] A. Quarteroni, A. Valli, Numerical Approximation of Partial Differential Equations, Springer-Verlag Berlin, 1997.
- [3] S.N. Atluri, T. Zhu, A new meshless local Petrov-Galerkin (MLPG) approach in computational mechanics, Comput. Mech. 22 (2) (1998) 117–127
- [4] S. De, K. Bathe, The method of finite spheres, Comput. Mech. 25 (4) (2000) 329-345.
- [5] Y. Krongauz, T. Belytschko, Consistent pseudo-derivatives in meshless methods, Comput. Methods Appl. Mech. Engrg. 146 (3-4) (1997) 371–386.
- [6] J.-S. Chen, M. Hillman, M. Rüter, An arbitrary order variationally consistent integration for Galerkin meshfree methods, Internat. J. Numer. Methods Engrg. 95 (5) (2013) 387–418.
- [7] M. Hillman, J. Chen, Y. Bazilevs, Variationally consistent domain integration for isogeometric analysis, Comput. Methods Appl. Mech. Engrg. 284 (2015) 521–540.
- [8] E.J. Kansa, Multiquadrics—A scattered data approximation scheme with applications to computational fluid-dynamics—I surface approximations and partial derivative estimates, Comput. Math. Appl. 19 (8–9) (1990) 127–145.
- [9] E.J. Kansa, Multiquadrics—A scattered data approximation scheme with applications to computational fluid-dynamics—II solutions to parabolic, hyperbolic and elliptic partial differential equations, Comput. Math. Appl. 19 (8–9) (1990) 147–161.
- [10] N. Aluru, A point collocation method based on reproducing kernel approximations, Internat. J. Numer. Methods Engrg. 47 (6) (2000) 1083–1121.
- [11] F. Auricchio, L.B. Da Veiga, T. Hughes, A. Reali, G. Sangalli, Isogeometric collocation methods, Math. Models Methods Appl. Sci. 20 (11) (2010) 2075–2107.
- [12] H.-Y. Hu, J.-S. Chen, W. Hu, Error analysis of collocation method based on reproducing kernel approximation, Numer. Methods Partial Differential Equations 27 (3) (2011) 554–580.
- [13] J.-S. Chen, M. Hillman, S.-W. Chi, Meshfree methods: progress made after 20 years, J. Eng. Mech. 143 (4) (2017) 04017001.
- [14] T.J. Hughes, J.A. Cottrell, Y. Bazilevs, Isogeometric analysis: CAD, finite elements, NURBS, exact geometry and mesh refinement, Comput. Methods Appl. Mech. Engrg. 194 (39–41) (2005) 4135–4195.
- [15] S.R. Idelsohn, E. Onate, Finite volumes and finite elements: two 'good friends', Internat. J. Numer. Methods Engrg. 37 (19) (1994) 3323–3341.
- [16] P. Cardiff, I. Demirdžić, Thirty years of the finite volume method for solid mechanics, Arch. Comput. Methods Eng. (2021) 1-60.
- [17] S. Atluri, T.-L. Zhu, The meshless local Petrov-Galerkin (MLPG) approach for solving problems in elasto-statics, Comput. Mech. 25 (2) (2000) 169–179.
- [18] S. Atluri, S. Shen, The meshless local Petrov-Galerkin (MLPG) method: A simple & less-costly alternative to the finite element and boundary element methods, CMES Comput. Model. Eng. Sci. 3 (1) (2002) 11–52.

- [19] S. Long, K. Liu, D. Hu, A new meshless method based on MLPG for elastic dynamic problems, Eng. Anal. Bound. Elem. 30 (1) (2006) 43–48.
- [20] Z. Han, S. Atluri, A meshless local Petrov-Galerkin (MLPG) approach for 3-dimensional elasto-dynamics, CMC: Comput. Mater. Contin. 1 (2) (2004) 129–140.
- [21] P. Wen, M. Aliabadi, An improved meshless collocation method for elastostatic and elastodynamic problems, Commun. Numer. Methods. Eng. 24 (8) (2008) 635–651.
- [22] F. Auricchio, L.B. Da Veiga, T.J. Hughes, A. Reali, G. Sangalli, Isogeometric collocation for elastostatics and explicit dynamics, Comput. Methods Appl. Mech. Engrg. 249 (2012) 2–14.
- [23] S. Chi, J. Chen, H. Luo, H. Hu, L. Wang, Dispersion and stability properties of radial basis collocation method for elastodynamics, Numer. Methods Partial Differential Equations 29 (3) (2013) 818–842.
- [24] B. Nayroles, G. Touzot, P. Villon, Generalizing the finite element method: Diffuse approximation and diffuse elements, Comput. Mech. 10 (5) (1992) 307–318.
- [25] S. Li, W.K. Liu, Moving least-square reproducing kernel method part II: Fourier analysis, Comput. Methods Appl. Mech. Engrg. 139 (1–4) (1996) 159–193.
- [26] M. Bessa, J. Foster, T. Belytschko, W.K. Liu, A meshfree unification: Reproducing kernel peridynamics, Comput. Mech. 53 (6) (2014) 1251–1264.
- [27] H. Zhang, D. Wang, Reproducing kernel formulation of B-spline and NURBS basis functions: A meshfree local refinement strategy for isogeometric analysis, Comput. Methods Appl. Mech. Engrg. 320 (2017) 474–508.
- [28] D. Wang, J. Wang, J. Wu, Superconvergent gradient smoothing meshfree collocation method, Comput. Methods Appl. Mech. Engrg. 340 (2018) 728–766.
- [29] D. Wang, J. Wang, J. Wu, Arbitrary order recursive formulation of meshfree gradients with application to superconvergent collocation analysis of Kirchhoff plates, Comput. Mech. 65 (3) (2020) 877–903.
- [30] Y. Leng, X. Tian, J.T. Foster, Super-convergence of reproducing kernel approximation, Comput. Methods Appl. Mech. Engrg. 352 (2019) 488–507.
- [31] D. Wang, D. Qi, X. Li, Superconvergent isogeometric collocation method with Greville points, Comput. Methods Appl. Mech. Engrg. 377 (2021) 113689.
- [32] W.K. Liu, S. Jun, Y.F. Zhang, Reproducing kernel particle methods, Internat. J. Numer. Methods Fluids 20 (8-9) (1995) 1081-1106.
- [33] J.-S. Chen, C. Pan, C.-T. Wu, W.K. Liu, Reproducing kernel particle methods for large deformation analysis of non-linear structures, Comput. Methods Appl. Mech. Engrg. 139 (1–4) (1996) 195–227.
- [34] J. Wu, D. Wang, An accuracy analysis of Galerkin meshfree methods accounting for numerical integration, Comput. Methods Appl. Mech. Engrg. 375 (2021) 113631.
- [35] S. Beissel, T. Belytschko, Nodal integration of the element-free Galerkin method, Comput. Methods Appl. Mech. Engrg. 139 (1-4) (1996) 49-74.
- [36] J.-S. Chen, C.-T. Wu, S. Yoon, Y. You, A stabilized conforming nodal integration for Galerkin mesh-free methods, Internat. J. Numer. Methods Engrg. 50 (2) (2001) 435–466.
- [37] N.M. Newmark, A method of computation for structural dynamics, J. Eng. Mech. Div. 85 (3) (1959) 67-94.